REPUBLIQUE ALGERIENNE DEMOCRATIQUE ET POPULAIRE
MINISTERE DE L'ENSEIGNEMENT SUPERIEUR ET DE LA RECHERCHE SCIENTIFIQUE
Université de Mohamed El-Bachir El-Ibrahimi - Bordj Bou Arreridj
Faculté *des Sciences et de la technologie*
Département Electromécanique

Mémoire

Présenté pour obtenir
LE DIPLOME DE MASTER
FILIERE : Electromécanique
Spécialité: Energie Renouvelables
Par

➢ **Dahmani Houssam Eddine**

Intitulé

Implémentation du control MPPT pour les systèmes photovoltaïques sur dSPACE

Implementation of MPPT Control for Photovoltaic Systems on dSPACE

Soutenu le: 02/07/2025

Devant le Jury composé de :

Nom & Prénom	*Grade*	*Qualité*	*Etablissement*
M. A. BENHENICHE	*MCA*	*Président*	*Univ-BBA*
M. F. ZEBIRI	*MCA*	*Encadreur*	*Univ-BBA*
M. A. Kessal	*Pr*	*Examinateur*	*Univ-BBA*
M. A. CHOUDAR	*MCB*	*Invité*	*Univ-BBA*

Année Universitaire 2024/2025

بسم الله الرحمن الرحيم

Acknowledgment

First and foremost, all praise and gratitude are due to God Almighty for the strength and opportunity to complete this thesis.

I wish to express my most sincere gratitude to my supervisor, ***Mr. F. ZEBIRI***, for his invaluable guidance and unwavering support throughout this research journey.

Special thanks are extended to **Mr. A. CHOUDAR** and **Mr. S. S. Merwan** for providing the necessary equipment for the experimental validation.

My deepest thanks are also extended to my family for their support, encouragement, and prayers.

Dedication

To my parents,

who first instilled in me a love for knowledge and the courage to pursue it.

Abstract

This thesis presents a comprehensive framework for the design, simulation, and experimental validation of MPPT control system for PV applications. The system utilizes a DC-DC boost converter to interface a PV panel with a load, ensuring optimal power extraction under varying environmental conditions. The work begins with the theoretical modeling of the PV panel using the single-diode model and the boost converter using the state-space averaging method. A study is then conducted between two Perturb and Observe (P&O) MPPT strategies: a direct control method and a control method employing a cascaded PI control structure. Simulations performed demonstrated the functional capabilities of both methods, with the cascaded controller showing superior dynamic performance and robustness to load disturbances. These findings are then rigorously verified through experimental tests on a physical test bench. A dSPACE DS1104 board is used as a real-time controller to implement the algorithms.

Keywords: Photovoltaic (PV), DC-DC Boost Converter, MPPT, experimental validation.

ملخص

تقدم هذه الأطروحة إطارًا شاملًا لتصميم ومحاكاة والتحقق التجريبي لنظام تحكم MPPT لتطبيقات الطاقة الشمسية. يستخدم النظام محولًا Boost DC-DC لربط لوحة طاقة شمسية بحمل، مما يضمن استخراج الطاقة المثلى تحت ظروف بيئية متغيرة. يبدأ العمل بالنمذجة النظرية للوحة الطاقة الشمسية باستخدام نموذج الصمام الواحد، ومحول Boost باستخدام طريقة متوسط مساحة الحالة. بعد ذلك، يتم إجراء دراسة مقارنة بين استراتيجيتين لتتبع نقطة الطاقة القصوى :طريقة التحكم المباشر(P&O) وطريقة تحكم تستخدم هيكل تحكم PI متتالي. أظهرت عمليات المحاكاة القدرات الوظيفية لكلا الأسلوبين، مع تفوق المتحكم المتتالي في الأداء الديناميكي والقدرة على تحمل اضطرابات الحمل. ثم تم التحقق من هذه النتائج بدقة من خلال الاختبارات التجريبية على منصة اختبار فعلية. تم استخدام لوحة dSPACE DS1104كمتحكم في الوقت الحقيقي لتنفيذ الخوارزميات .

الكلمات المفتاحية: الطاقة الشمسية (PV)، محول Boost DC-DC، تتبع نقطة الطاقة القصوى (MPPT)، التحقق التجريبي.

Résumé:

Cette thèse présente un cadre complet pour la conception, la simulation et la validation expérimentale d'un système de contrôle MPPT pour les applications photovoltaïques. Le système utilise un convertisseur DC-DC boost pour interfacer un panneau PV avec une charge, assurant une extraction optimale de la puissance dans des conditions environnementales variables. Le travail commence par la modélisation théorique du panneau photovoltaïque à l'aide du modèle à diode unique et du convertisseur élévateur à l'aide de la méthode de calcul de la moyenne de l'espace d'état. Une étude est ensuite menée entre deux stratégies de perturbation et d'observation (P&O) MPPT : une méthode de contrôle direct et une méthode de contrôle utilisant une structure de contrôle PI en cascade. Les simulations effectuées ont démontré les capacités fonctionnelles des deux méthodes, le contrôleur cascadé montrant des performances dynamiques supérieures et une robustesse aux perturbations de la charge. Ces résultats sont ensuite rigoureusement vérifiés par des tests expérimentaux sur un banc d'essai physique. Une carte dSPACE DS1104 est utilisée comme contrôleur en temps réel pour implémenter les algorithmes.

.**Mots-clés :** Photovoltaïque (PV), convertisseur DC-DC Boost, MPPT, validation expérimentale

List of Abbreviations

List of Symbols

List of Tables

List of Figures

Contents

Contents

Contents

General Introduction

I. General Introduction

The escalating global demand for energy, coupled with the significant environmental concerns associated with the combustion of fossil fuels, has intensified the search for clean and sustainable energy alternatives. Renewable energy sources, particularly solar energy, are recognized as critical technologies for a sustainable future due to their abundance and environmentally benign nature [1]. Photovoltaic (PV) systems, which directly convert sunlight into electricity, represent one of the most promising avenues for harnessing this renewable resource. The fundamental component of these systems is the photovoltaic cell, a specially designed semiconductor p-n junction where incident photons with sufficient energy create electron-hole pairs, thereby generating an electric current [2].

However, the widespread adoption of PV technology is hindered by two primary challenges: relatively low conversion efficiency and the non-linear output characteristics of PV modules. The power generated by a PV panel is highly dependent on fluctuating environmental conditions, primarily solar irradiance and temperature [3]. This results in a unique but constantly shifting Maximum Power Point (MPP) on the panel's power-voltage (P-V) curve [4]. To maximize the energy yield and ensure the economic viability of a PV system, it is crucial to force the panel to operate continuously at this optimal point. This fundamental challenge is known as the "problem of optimization" in photovoltaic systems.

The solution to this problem lies in the implementation of a Maximum Power Point Tracking (MPPT) algorithm. These algorithms are executed by a power electronic interface, typically a DC-DC converter, which is placed between the PV array and the load [5]. By dynamically adjusting the converter's duty cycle, the MPPT controller effectively modifies the impedance seen by the PV panel, ensuring it operates at its MPP regardless of environmental variations. Numerous MPPT techniques have been proposed, with conventional methods like Perturb and Observe (P&O) and Incremental Conductance (IncCond) being widely used due to their simplicity and effectiveness [6].

This thesis presents a comprehensive study of the design, modeling, simulation, and experimental validation of an MPPT control system for a photovoltaic energy conversion chain. The work is structured to bridge the gap from fundamental theory to practical hardware implementation.

Chapter 1 establishes the theoretical foundations of photovoltaic systems. It details the photovoltaic effect, the electrical modeling of PV panels based on the single-diode model, and analyzes their characteristic curves under varying conditions. It then introduces the concept of the Maximum Power Point and provides a survey of various MPPT techniques used to track it.

Chapter 2 delves into the critical power electronic interface: the DC-DC boost converter. This chapter focuses on the detailed mathematical modeling of the converter using the state-space averaging method. It then presents a comparative simulation study of two PO MPPT control strategies; a direct MPPT method and a control MPPT method to evaluate their performance in tracking the MPP under dynamic load conditions.

Chapter 3 transitions from simulation to practice by presenting the experimental validation of the developed control schemes. Utilizing a dSPACE DS1104 controller board in a Hardwar configuration, the MPPT algorithms are implemented and tested on a physical PV system. The experimental results are analyzed to verify the performance, efficiency, and robustness of the controllers in a real-world environment.

Ultimately, this work aims to provide a complete framework for the analysis and implementation of an efficient and reliable MPPT system, demonstrating the successful integration of theoretical principles with practical power electronics and control engineering.

Chapter I

Photovoltaic Systems and Power Optimization Techniques

I. Photovoltaic Systems and Power Optimization Techniques

I.1 Introduction

This chapter lays the foundational groundwork for understanding photovoltaic (PV) energy systems and the critical challenge of optimizing their power output. It begins by exploring the fundamental science, detailing the photovoltaic effect and the principles of energy conversion within solar cells. A significant focus is placed on modeling and characterizing PV panels, as their non-linear I-V and P-V characteristics under varying environmental conditions are central to the optimization problem.

The discussion then broadens to encompass practical system aspects, including common PV system configurations and PV-load connection methods. This contextualizes the environment in which optimization strategies operate. The chapter culminates by highlighting the importance of Maximum Power Point Tracking (MPPT) and introducing various MPPT techniques, thereby setting the stage for the detailed analysis and implementation explored in subsequent parts of this thesis.

I.2 The Photovoltaic Effect

The photovoltaic (PV) cell converts sunlight directly into electricity [2]. As the fundamental component of any PV power plant, its structure comprises two semiconductor layers: a P-type (positively doped) layer and an N-type (negatively doped) layer, forming a PN junction. To ensure good electrical contact, metal grids are placed on both sides of the cell. An anti-reflective coating is also added to minimize the loss of energy caused by sunlight reflecting off the surface.

The depletion region at the PN junction creates an electric field that separates light-generated charge carriers (electrons and holes). This separation prevents recombination and enables current flow through the external circuit Figure I.1.

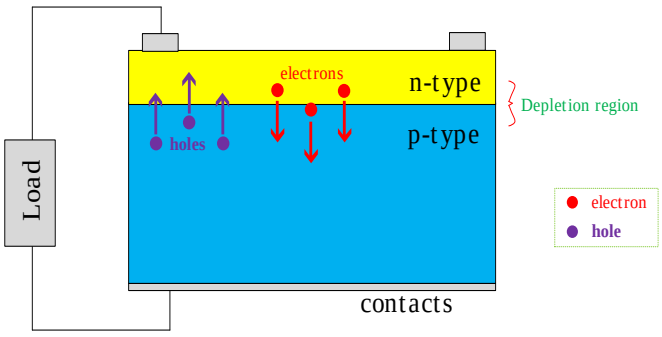

Figure I.1 Photovoltaic Cell Structure [2]

I.3 Principle of Photovoltaic Energy Conversion

Three key requirements govern solar power generation:

1. **Photon Absorption**: A material (e.g., silicon) must absorb sunlight to create electron-hole pairs.
2. **Charge Separation**: The PN junction's electric field separates carriers, driving electrons to the N-type layer and holes to the P-type layer.
3. **Voltage Generation**: The built-in potential at the junction produces a usable voltage (~0.5–0.7 V for silicon) [2].

For electricity to be generated, the incoming sunlight must have a minimum level of energy, known as the material's 'bandgap' When photons strike the cell with energy above this threshold, they free electrons to move through the material. The electric field sweeps these carriers across the junction, creating a current (Figure I.2).

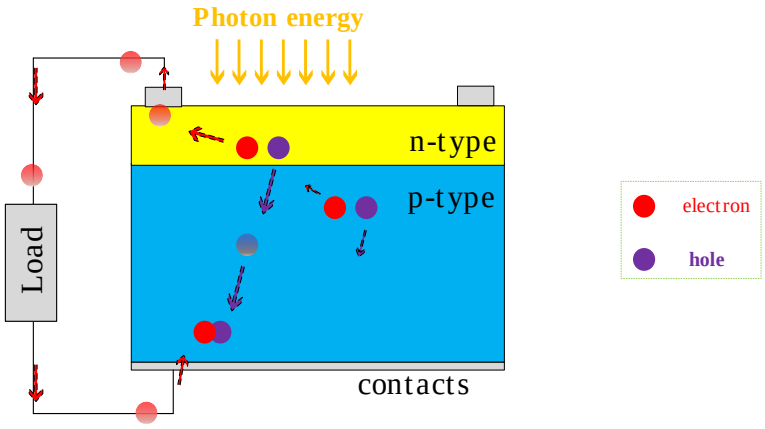

Figure I.2 PV Cell Operation [2]

I.4 Modeling and Characteristics of PV Panels

The performance of photovoltaic (PV) systems relies fundamentally on the PV cell, the basic unit responsible for converting solar energy into electrical energy. Accurate modeling of the PV cell is essential for simulating system behavior, designing efficient power electronics, and implementing maximum power point tracking (MPPT) control strategies, such as those tested in hardware mode using dSPACE in this thesis.

I.4.1 Single-Diode Model

The single-diode model simplifies PV cell analysis while balancing accuracy and complexity[3]:

$$I = I_{Ph} - I_D(V) \tag{1.1}$$

- I_{Ph} : Light-generated current (proportional to irradiance).
- I_D : Diode current representing recombination losses.

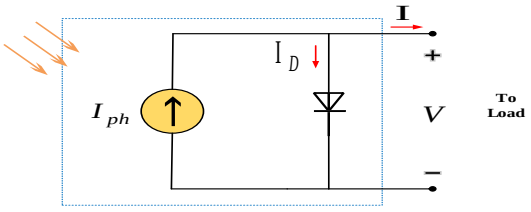

Figure I.3 Ideal PV Cell Model [3]

The electrical behavior of a PV cell is significantly influenced by the diode it incorporates, modeled using the Shockley diode equation[3]. The diode current I_D is expressed as:

$$I_D = I_O \left(e^{\frac{QV_D}{kT}} - 1 \right) \quad (1.2)$$

where:

- I_D: Diode current (A),
- I_0: Reverse saturation current (A),
- q: Elementary charge (1.6×10^{-19}C),
- V_D: Voltage across the diode (V),
- k: Boltzmann's constant (1.38×10^{-23}J/K),
- T: Absolute temperature (K).

The reverse saturation current I_0 is a critical parameter, strongly dependent on temperature. For silicon-based PV cells near room temperature (approximately 300 K), I_0 doubles for every 10°C increase, reflecting the material's sensitivity to thermal variations [7]. This temperature dependence affects the diode's current-voltage (I-V) characteristics, as shown in Figure I.4, which plots I_D versus V_D at 300 K and 350 K. At 300 K, I_0 is approximately 50 nA, but it increases significantly at higher temperatures, affecting the cell's performance under varying environmental conditions [8].

The term $\frac{kT}{q}$, known as the thermal voltage V_{th}, simplifies the equation when analyzing operating conditions. At 300 K with a=1, $V_{th} \approx$ 25.84 mV. For diode voltages $V_D \gg V_{th}$ (e.g., 50–60 mV), the exponential term dominates, rendering the "-1" negligible under typical PV operating conditions [2].

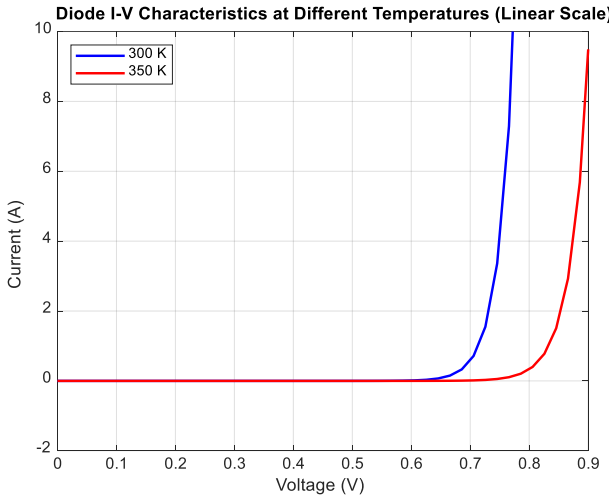

Figure I.4 Diode I-V Characteristics at Different Temperatures

I.4.2 Ideal PV Cell Model

The ideal PV cell model combines a photon-generated current source I_{ph} in parallel with the diode[3]:

$$I = I_{ph} - I_D = I_{ph} - I_0\left(\exp\left(\frac{qV}{akT}\right) - 1\right) \quad (1.3)$$

Real PV cells exhibit non-idealities, modeled by adding series resistance R_s and shunt resistance R_{sh}.

- **Series Resistance** (R_s): Accounts for resistive losses in the cell's contacts, metal grid, and semiconductor layers (P-type and N-type). The modified equation becomes:

$$I = I_{ph} - I_0\left(\exp\left(\frac{q(V + IR_s)}{akT}\right) - 1\right) \quad (1.4)$$

Here, the diode voltage $V_D = V + IR_s$ reflects the voltage drop across R_s. This resistance impacts the I-V curve's slope near the open-circuit voltage, reducing the maximum power output.

- **Shunt Resistance** (R_{sh}): Represents leakage currents across the PN junction, often due to manufacturing defects or poor material quality. The complete single-diode model is:

$$I = I_{ph} - I_0\left(\exp\left(\frac{q(V + IR_s)}{akT}\right) - 1\right) - \frac{V + IR_s}{R_{sh}} \quad (1.5)$$

A high R_{sh} (typical of quality cells) minimizes leakage, while low values indicate defective cells, with power losses more pronounced at low irradiance levels due to a larger proportion of I_{ph} being diverted through R_{sh}.

The equivalent circuit, including the Diode, I_{ph}, R_s, and R_{sh} is depicted in Figure I.5.

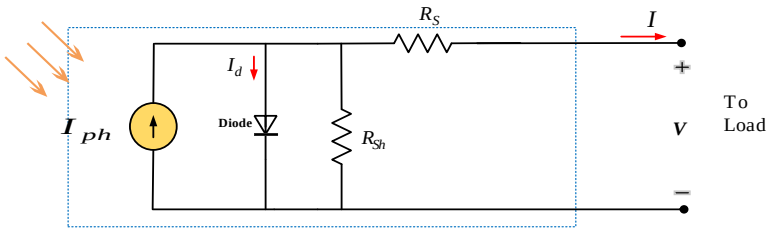

Figure I.5 PV Cell Model with Series and Shunt Resistance [9] [3]

I.4.3 I-V and P-V Characteristics under Environmental Conditions

The following analysis is based on the "Sunway Solar SW360M-60" module, which is also the subject of the experimental work in Chapter 3. Key parameters for the single-diode model were extracted from the manufacturer's datasheet [10] to ensure simulation accuracy. These parameters include a series resistance (R_s) of 0.28 Ω, a shunt resistance (R_{sh}) of 559.25 Ω, and a diode ideality factor (a) of 1.06. This approach allows for a direct comparison between the simulated and empirical results.

Table A Sunway Solar SW360M-60 PV panel characteristics at STC (appendix B).

Maximum power, Pmax	320 W (0-+5W)
Open circuit voltage, V_{OC}	41.00 V
Short circuit current, I_{SC}	10.14 A
Temperature coefficient of current, Ki	+0.059%/°C
Temperature coefficient of voltage, Kv	-0.330%/°C
Maximum power voltage	33.40 V
Maximum power current	9.58 A

I.4.3.1 **I-V Characteristics**

Figure I.6(a) presents the current-voltage (I-V) characteristics of the solar module at different temperatures while maintaining a constant irradiation level $1000W/m^2$. As the temperature increases, the open-circuit voltage (V_{oc}) decreases, and the short-circuit current (I_{sc}) shows a slight increase. This behavior is consistent with the temperature dependence of photovoltaic devices, where higher temperatures lead to a reduction in the bandgap energy, thereby decreasing V_{oc}, and a minor increase in I_{sc} due to enhanced carrier generation.

Figure I.7 (a) displays the I-V characteristics of the solar module under different levels of solar irradiation at a constant temperature 25°C. With increasing irradiation, both the short-circuit current (I_{sc}) and the open-circuit voltage (V_{oc}) increase. The increase in I_{sc} is more significant, as it is directly proportional to the incident light intensity,V_{oc} while increases logarithmically with irradiation.

I.4.3.2 **P-V Characteristics**

Figure I.6 (b) illustrates the power-voltage (P-V) characteristics under the same temperature conditions. The maximum power point (P_{max}) decreases as temperature increases, indicating a reduction in the module's efficiency at higher temperatures.

Figure I.7 (b) shows the P-V characteristics for varying solar irradiations. The maximum power point (P_{max}) increases with higher irradiation levels, reflecting the greater power output achievable under stronger sunlight.

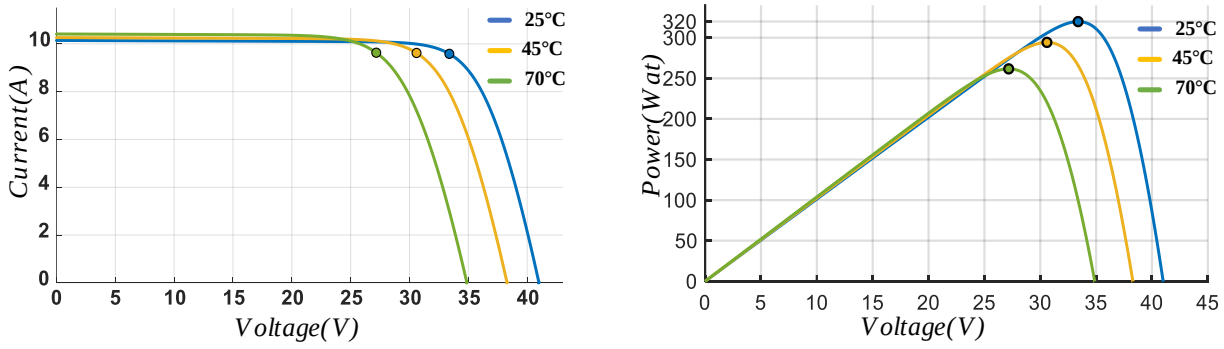

Figure I.6 (a) I-V and (b) P-V Characteristics of a Solar Module Under Varying temperature

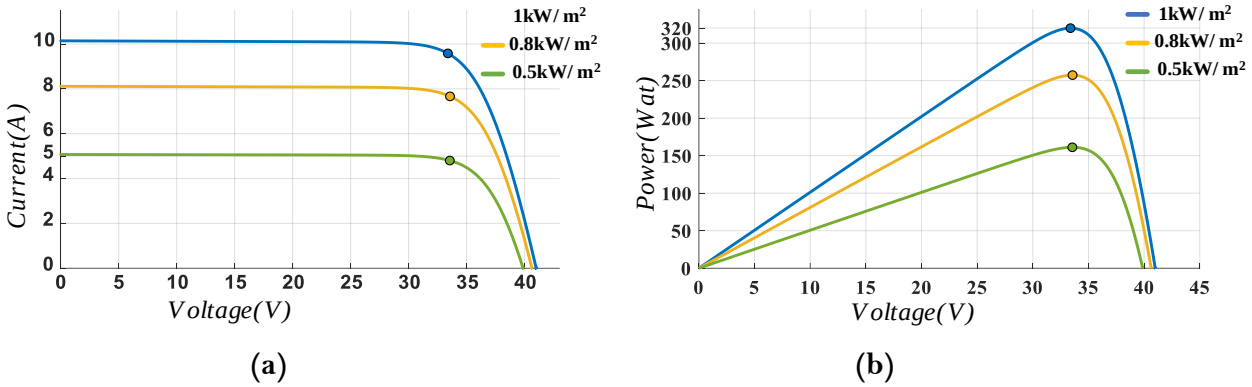

Figure I.7 (a) I-V and (b) P-V Characteristics of a Solar Module Under Varying Solar Irradiations

I.5 PV System Configurations

Photovoltaic (PV) systems are broadly classified into *standalone* and *grid-connected* configurations, each with distinct design philosophies and applications [5]. This section outlines the most widely adopted configurations, focusing on their structural and operational characteristics.

I.5.1 Standalone PV Systems

Standalone systems operate independently of the utility grid and are typically deployed in remote or off-grid applications [5]. These systems require energy storage (e.g., batteries) to ensure continuous power supply during periods of low solar irradiance.

I.5.1.1 DC Load Systems

Standalone PV systems supporting DC loads (e.g., streetlights, water pumps, or mobile devices) consist of a PV array, charge controller, battery bank, and DC-DC converter (Figure I.8). The charge controller regulates battery charging, while the DC-DC converter ensures stable voltage delivery to the load. These systems are cost-effective for low-power applications where AC power is unnecessary.

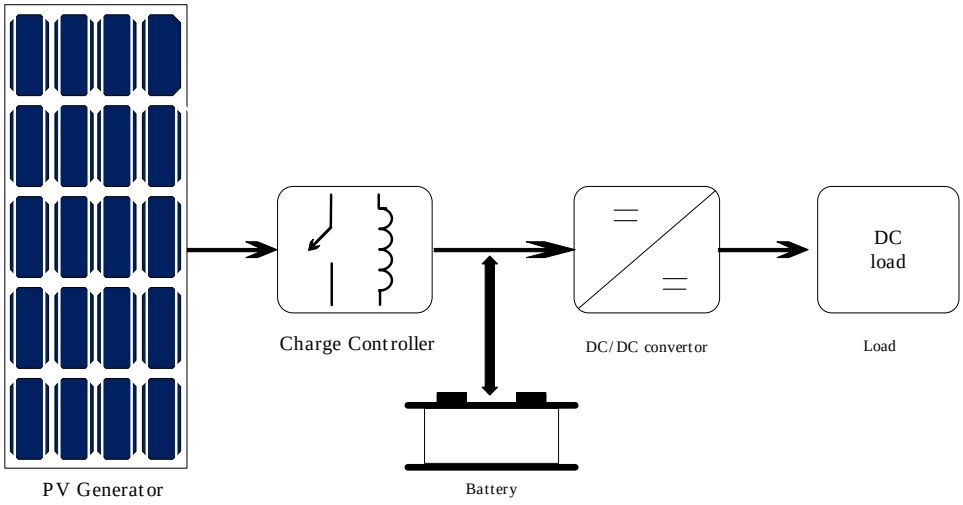

Figure I.8 Standalone PV system with DC load, battery storage, and charge controller [5].

I.5.1.2 AC Load Systems

For AC loads (e.g., household appliances), standalone systems incorporate a DC-AC inverter to convert battery-stored DC power into grid-quality AC power (Figure I.9). Hybrid configurations may integrate backup generators (e.g., diesel) to enhance reliability during prolonged low-solar conditions.

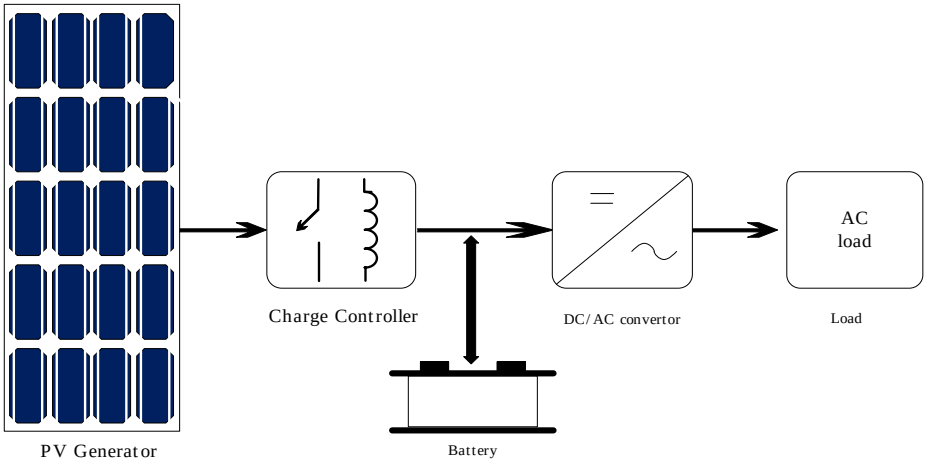

Figure I.9 Standalone PV system with AC load, inverter, and hybrid generator support [5].

I.5.2 Grid-Connected PV Systems

Grid-connected systems dominate the PV market due to their scalability and ability to feed surplus energy into the utility grid. Three primary configurations exist:

I.5.2.1 Central Inverter Systems

Central inverters are used in utility-scale installations (>250 kW). Multiple PV strings (series-connected panels) are paralleled into a large DC array, converted to AC via a single high-power inverter (Figure I.10). While cost-effective and efficient (>97%), central inverters suffer from reduced energy yield under partial shading or panel mismatch due to a single maximum power point tracking (MPPT) unit.

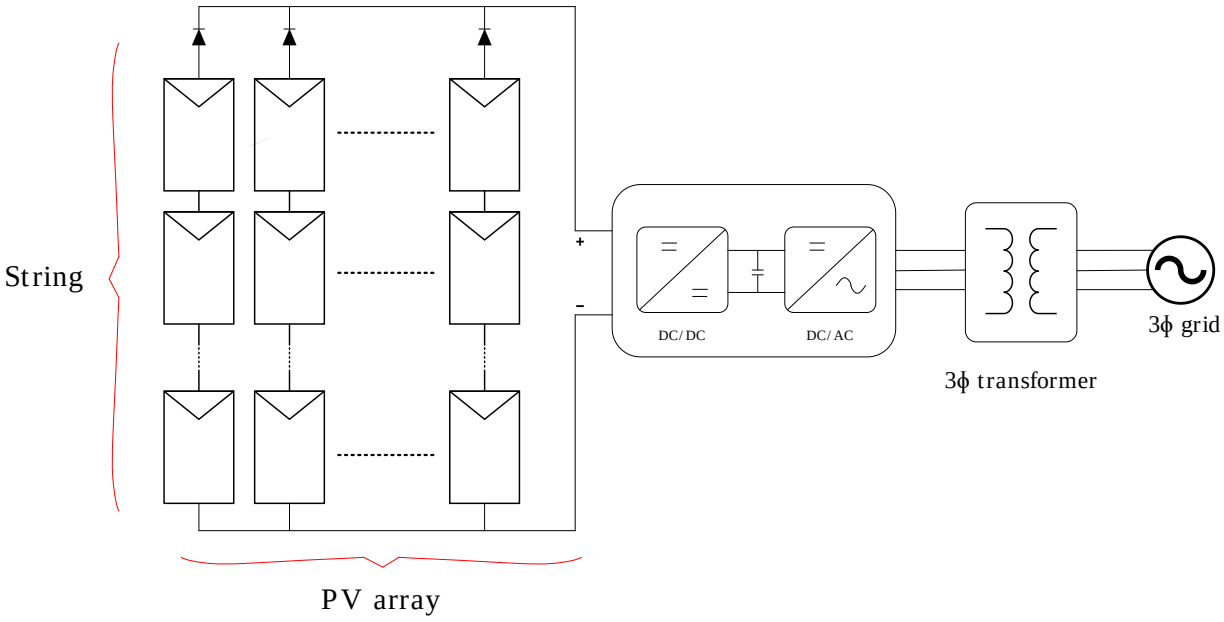

Figure I.10 Central inverter system with parallel PV strings and grid interface via a step-up transformer [5].

I.5.2.2 String Inverter Systems

String inverters (2–10 kW) are common in residential applications. Each PV string connects to a dedicated inverter, enabling per-string MPPT (Figure I.11). This design improves energy yield under

shading compared to central inverters. Modern string inverters often use transformerless topologies, reducing cost and weight while complying with evolving grid codes.

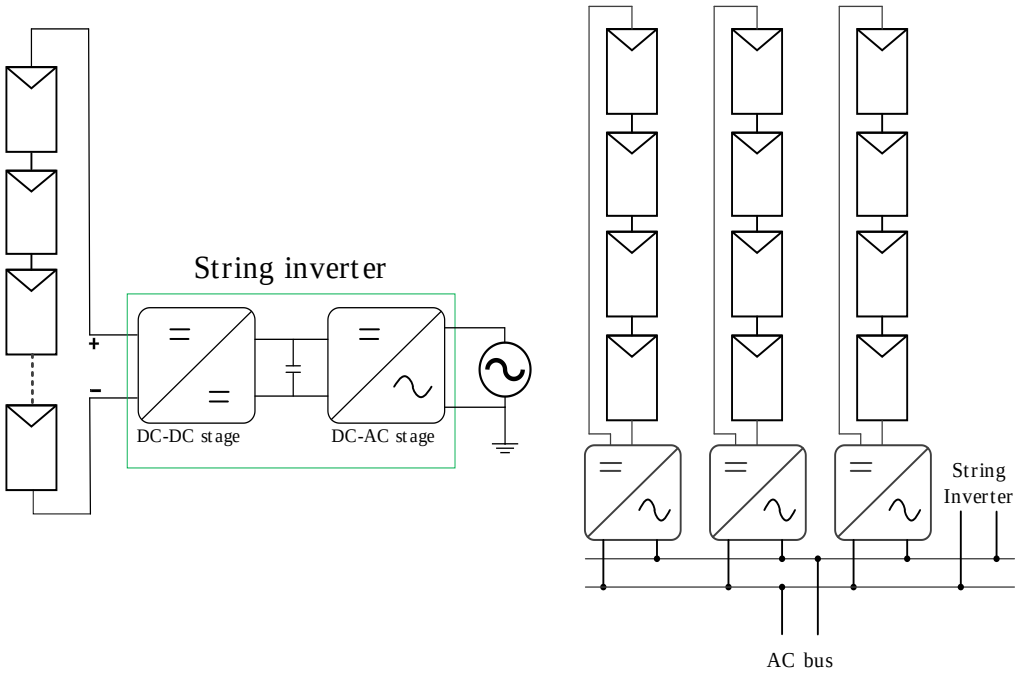

Figure I.11 String inverter system with individual MPPT per string and transformerless grid interface [5].

I.5.2.3 Microinverter Systems

Microinverters (200–300 W) attach directly to individual panels, enabling per-panel MPPT (Figure I.12). This configuration maximizes energy harvest in partially shaded or mismatched arrays and eliminates high-voltage DC wiring. Though less efficient (94–96%) and costlier per watt, microinverters offer modularity and simplified system expansion.

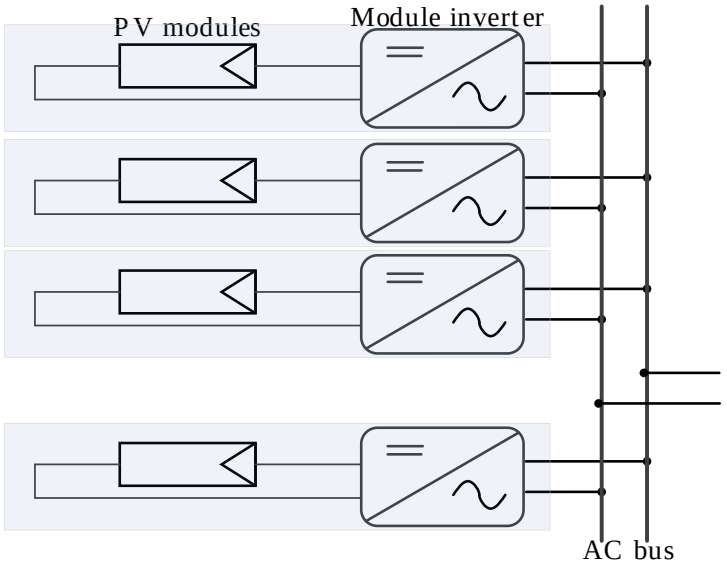

Figure I.12 Microinverter system with per-panel MPPT and direct AC grid coupling [5].

I.6 PV-Load Coupling and Power Electronics

I.6.1 Role of DC-DC Converters

The principal role of DC-DC converters lies in their application as switching power supplies. A key advantage they offer is high conversion efficiency, which enables a greater power packing density. This density can be further improved by increasing the converter's switching frequency, as this allows for a reduction in the physical size and weight of the required energy storage components. Moreover, the fundamental on-off switching action of the converter's transistor inherently minimizes the power losses that are characteristic of linear regulation methods. Beyond their use in power supplies, these converters are also integral to the control of direct-current (DC) motor drives, a context in which they are frequently referred to as "choppers" [11].

I.6.2 Role of Inverter

Inverter systems are categorized by grid connectivity, power phase (single/three-phase), and isolation mechanisms (transformer-base / transformerless). Grid-connected inverters dominate the market, often utilizing line-frequency transformers for voltage step-up in utility-scale applications. Emerging standards have popularized transformerless designs, particularly in residential settings. Configurations further include central inverters (for large arrays), string inverters (per-series strings), and microinverters (per-panel), each tailored to specific scalability and efficiency requirements.

I.7 Maximum Power Point Tracking (MPPT)

The I-V curve of a PV module features a singular maximum power point (MPP), which shifts with environmental conditions [12]. Power electronic converters, governed by MPPT algorithms, ensure continuous operation at this optimal point, mitigating energy losses caused by nonlinearities.

I.7.1 Importance of MPPT

To optimize the energy yield of a photovoltaic (PV) system, it is crucial to ensure the PV array operates at its peak power output. Therefore, the implementation of a Maximum Power Point Tracking (MPPT) algorithm is a critical and indispensable function in the system's power electronics interface [6]. This technique is vital for adapting to fluctuating irradiance and temperature levels, thereby maximizing the overall efficiency and energy generation of the system.

I.7.2 Different Types of MPPT

The Maximum Power Point Tracking (MPPT) techniques discussed in the following subsections provides detailed classifications, operational principles, and comparative analyses of various MPPT methods [1].

I.7.2.1 Direct MPPT Methods

Direct Maximum Power Point Tracking (MPPT) methods determine the MPP exclusively through real-time measurements of the PV array's voltage and current. The goal is to drive the system towards the peak of the P-V curve, where the derivative of power with respect to voltage ($\frac{dP}{dV}$) is zero. Their defining characteristic is that they do not require any prior knowledge of the panel's characteristics or measurements of environmental data like solar irradiance or temperature [6].

A. Hill Climbing (HC) Technique

This method gets its name from the "hill-shaped" form of the PV panel's power-voltage (P-V) curve. The algorithm works by making small adjustments to a control variable and observing the effect on the output power, iteratively "climbing" towards the peak. While effective, its main drawback is the risk of getting trapped at a local maximum power point, especially under partial shading conditions.

The size of the adjustment, or perturbation step (S), determines the trade-off between tracking speed and steady-state stability :

$$S = \frac{DP / DD}{P / D} \tag{1.6}$$

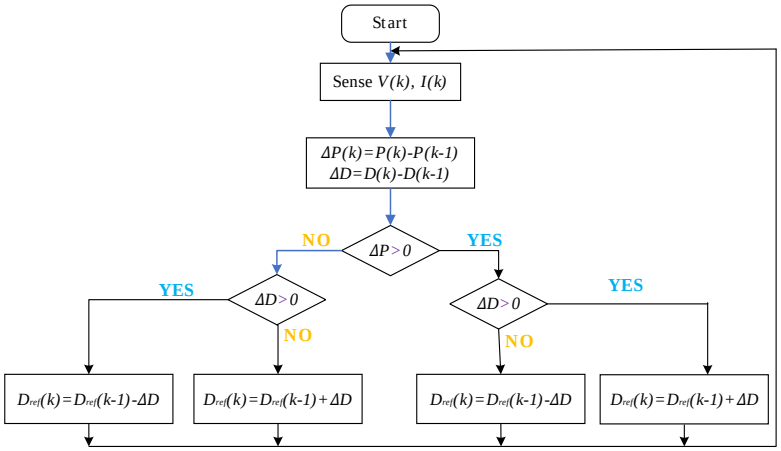

Figure I.13 Hill Climbing Flowchart [13].

B. Fuzzy Logic Control

A fuzzy logic controller operates through a distinct, multi-stage process designed to translate numerical data into intelligent action, as illustrated in Figure I.14. The initial stage, known as fuzzification, involves translating precise numerical inputs (crisp values) from sensors into linguistic variables defined by membership functions. Following this, an inference engine evaluates these fuzzy inputs against a pre-defined rule base. This rule base consists of a series of 'if-then' statements that codify the desired relationship between the system's inputs and outputs. The final stage is defuzzification, where the fuzzy output generated by the inference engine is converted back into a single, actionable crisp value that can be used to control a physical component [14].

This approach uses fuzzy rules to handle the PV system's complexities, adapting to changes. It can be quick and accurate but needs expert setup and is computationally heavy.

$$\begin{cases} E(i) = \dfrac{P_{pv}(i) - P_{pv}(i-1)}{V_{pv}(i) - V_{pv}(i-1)}, \\ DE(i) = E(i) - E(i-1). \end{cases} \tag{1.7}$$

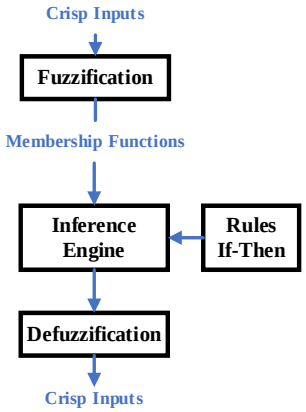

Figure I.14 Block diagram of a fuzzy logic control system [14].

C. Perturb and Observe (PO)

The direct Perturb and Observe (P&O) method is an MPPT algorithm that directly manipulates the duty cycle of the DC-DC converter. The algorithm works by introducing a small, fixed-step change to the duty cycle and observing the resulting effect on the PV array's output power.

If a perturbation leads to an increase in power, the next perturbation is made in the same direction. If the power decreases, the direction is reversed. While simple to implement, this method has the disadvantage of causing oscillations around the maximum power point (MPP) during steady-state conditions, which results in some energy loss [15].

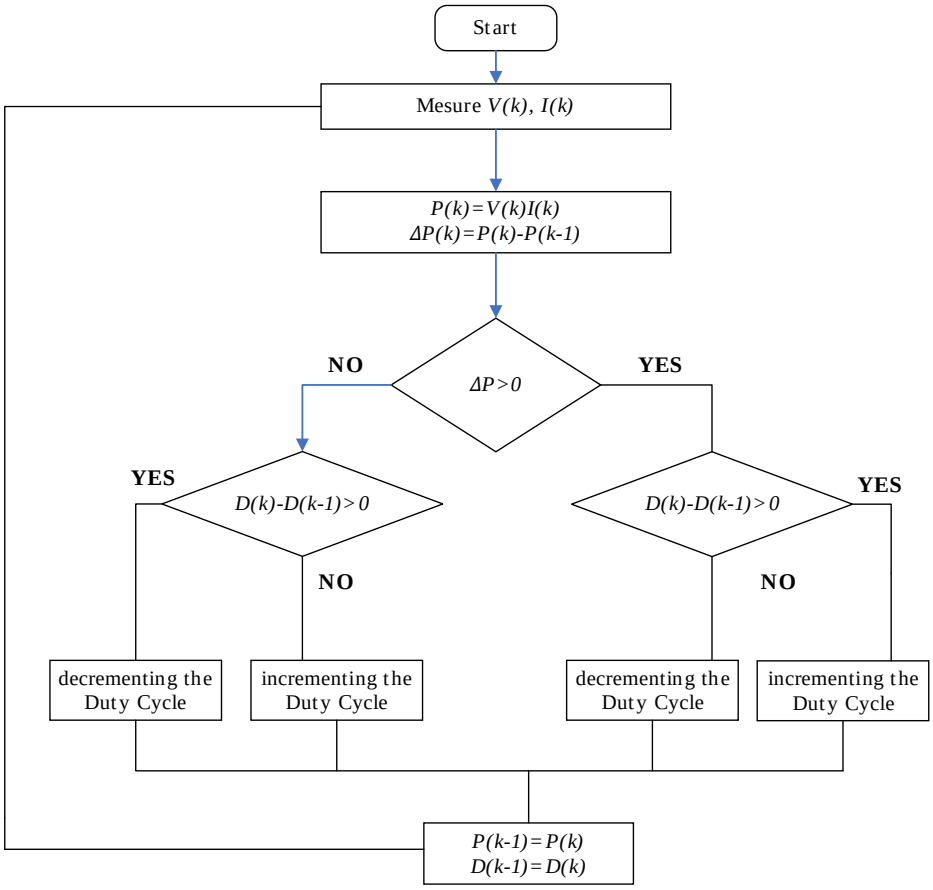

Figure I.15 PO direct method's flow diagram [15].

I.7.2.2 Indirect MPPT Methods

In contrast, indirect MPPT methods estimate the location of the MPP using a predefined mathematical model of the PV array. This model relies on empirical data and relationships, utilizing parameters such as the array's open-circuit voltage (V_{oc}) or short-circuit current (I_{sc}), often in combination with measurements of solar irradiance and cell temperature. Instead of iteratively searching for the MPP, the algorithm directly calculates an approximate operating point (V_{mpp} or I_{mpp}) and commands the power converter to operate there. While this approach can be faster and avoids the oscillations inherent in hill-climbing methods, its accuracy is fundamentally limited by the precision of the underlying model and the parameters used [6].

A. Fractional Open-Circuit Voltage (FOCV)

It guesses the best voltage as a fraction of the voltage when no current flows. It's simple and doesn't need current sensors, but it's less accurate and needs to stop power sometimes to measure, which isn't ideal.

$$(V_{MPP} = k \times V_{OC}), with\ (k \approx 0.72 - 0.8). \quad (1.8)$$

B. Fractional Short-Circuit Current (FSCC)

Similar to FOCV, it uses a fraction of the current when shorted. It's fast but needs extra hardware to measure, and accuracy depends on conditions.

$$(I_{MPP} = K_1 \times I_{SC}), with\ (K_1 \approx 0.78 - 0.92). \quad (1.9)$$

I.7.2.3 Control of MPPT

The MPPT technique tells a MPPT controller how to move the operating voltage. Then, it is a MPPT controller's task to bring the voltage to a desired level and maintain it. The proportional and integral (PI) controller regulates the input voltage of converter, Where the MPPT takes measurement of PV voltage and current and then taking algorithm calculates the reference voltage (V_{ref}) when the PV operating voltage should move next. The algorithm set to V_{ref} only, and repeated periodically with a slower rate. The PI controller task is minimize error between V_{ref} and the measured voltage by adjusting the duty cycle as shown in Figure I.16 [15].

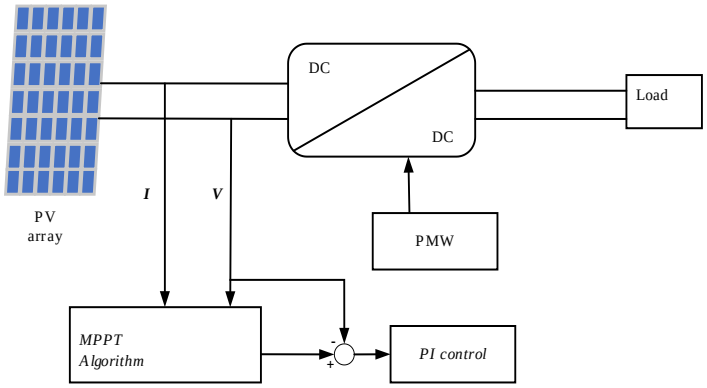

Figure I.16 Block diagram of PV generator systems with the PI controller

A. Perturb and Observe (PO)

MPPT is a critical technique in photovoltaic (PV) systems to ensure that the panels operate at their maximum power point (MPP), thereby optimizing energy harvesting. Indirect MPPT methods adjust the operating point based on real-time measurements of PV voltage and current. The Perturb and Observe (PO) algorithm is the most widely used direct MPPT method due to its simplicity and effectiveness under varying environmental conditions [4].

This simple method adjusts the voltage slightly and checks if power increases. If it does, it keeps going that way; if not, it reverses. It's easy to use but can wobble around the best power point, losing some energy, especially when the sun changes quickly.

$$\begin{cases} P(t) = V(t) \times I(t), \\ \Delta P = P(t) - P(t-1), \\ V(t) = V(t-1) \pm \Delta V. \end{cases} \quad (1.10)$$

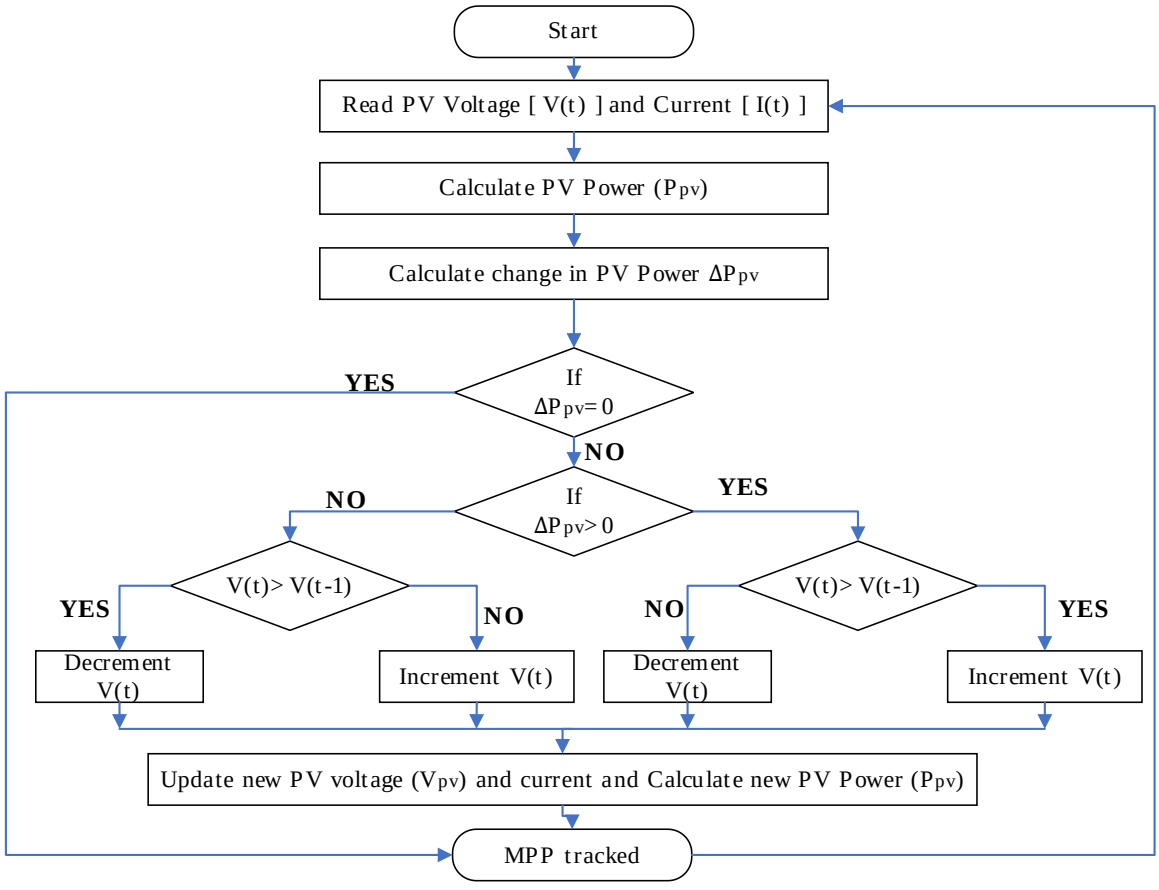

Figure I.17 PO Control method's flow diagram [1].

I.8 Conclusion

This chapter has provided a comprehensive overview of the fundamental principles governing photovoltaic systems and the critical importance of power optimization. Beginning with the core physics of the photovoltaic effect and energy conversion, the discussion progressed to the essential task of modeling a PV cell. The analysis of the single-diode model, including the effects of parasitic resistances, successfully established the non-linear relationship between a panel's voltage and current.

The resulting I-V and P-V characteristic curves clearly illustrated their strong dependency on environmental factors, namely solar irradiance and temperature.

The key takeaway from this analysis is the identification of the central challenge in PV energy harvesting: the existence of a singular, yet constantly shifting, Maximum Power Point (MPP). To address this, the chapter reviewed various PV system configurations and highlighted the indispensable role of power electronics. It was established that to maximize energy yield, a DC-DC converter governed by a sophisticated control algorithm is required to continuously operate the PV array at its MPP.

Finally, by introducing a spectrum of MPPT techniques—from foundational methods like Perturb and Observe (PO) to advanced strategies—this chapter has laid the necessary theoretical context. This groundwork is crucial for understanding the practical implementation of the PO algorithm, which is the central focus of the experimental work in this thesis. Having established why MPPT is necessary and what algorithms exist, the following chapters will now focus on the practical implementation. Chapter 2 will delve into the detailed analysis and modeling of the DC-DC boost converter, the power electronic actuator that makes these optimization strategies possible.

Chapter II

Modeling And Simulation of a Boost Converter Based PV MPPT System

II. Modeling and Simulation of a Boost Converter Based PV MPPT System

II.1 Introduction

Following the foundational understanding of photovoltaic systems established in Chapter 1, this chapter delves into the critical power electronic interface: the DC-DC converter. Essential for mediating between the variable output of a PV array and the requirements of a load or grid, DC-DC converters play a pivotal role in optimizing energy transfer, particularly through the implementation of Maximum Power Point Tracking (MPPT) algorithms. This chapter will focus on the comprehensive analysis, modeling, and foundational control aspects of these converters, with a specific emphasis on the boost converter topology, which is highly relevant for stepping up PV array voltages.

II.2 Analysis and Modeling of the DC-DC Boost Converter

A Boost converter, or parallel chopper, is a switching power supply that converts a continuous input voltage into a higher continuous output voltage [11].

It consists of a controlled switch S_1 (e.g., bipolar transistor, MOS transistor, or IGBT), an inductor L, a diode D_1, and an output capacitor C. The load is represented by the resistance R. The elements L and C form a filter designed to limit the ripple resulting from switching in the output voltage and current Figure II.1 [11], [16].

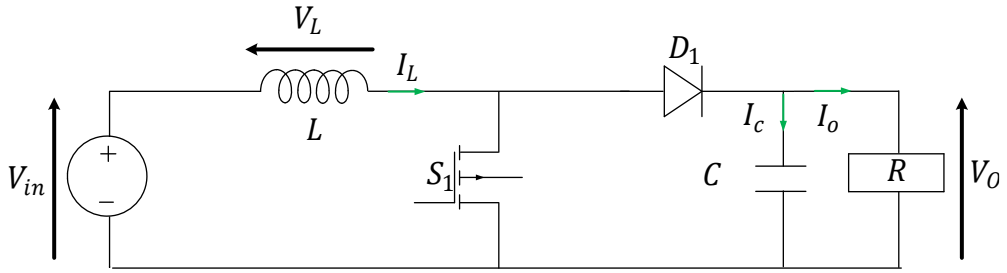

Figure II.1 Electrical Circuit Diagram of a Boost Converter

II.2.1 Dynamic Modeling of Boost Converter

Figure II.2 shows that when the controllable switch S_1 is turned on, the inductor L stores energy. When the switch S_1 is turned off, the inductor L releases its stored energy, charging the capacitor C and supplying the load R through the diode D_1 [11], [16]. When the switch S_1 is open and the diode conducts, the circuit can be represented as shown in the next figure. The state variables are the inductor current i_L as x_1 and the output voltage V_o as x_2.

A. *Closed switch:* On the interval $0 \le t \le dT$

The switch S_1 is closed, the diode D_1 is blocked, and the equivalent circuit is given in the following diagram Figure II.2 [11], [17].

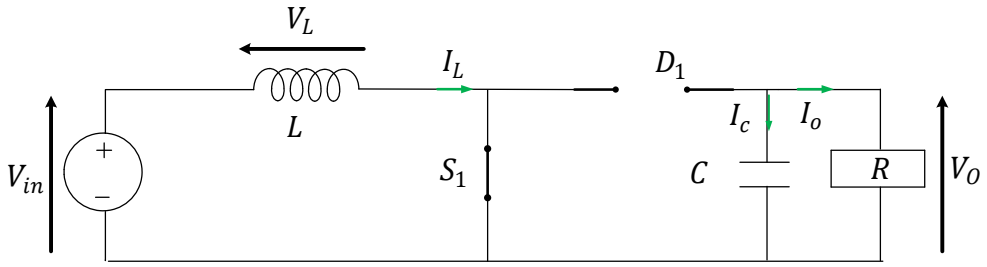

Figure II.2 S_1 switch is closed

Using Kirchhoff's Voltage Law around the input loop:

$$V_{in} - V_L = 0 \tag{II.11}$$

Thus:

$$V_{in}(t) = L \frac{di_L(t)}{dt} \tag{II.12}$$

$$\frac{di_L(t)}{dt} = \frac{V_{in}(t)}{L} \tag{II.13}$$

Kirchhoff's Current Law at the output node:

$$0 - i_C = i_o \tag{II.14}$$

Thus:

$$i_o(t) = -C \frac{dV_o(t)}{dt} \tag{II.15}$$

$$\frac{dV_o(t)}{dt} = -\frac{i_o(t)}{C} = -\frac{V_o(t)}{RC} \tag{II.16}$$

The differential equations are:

$$\begin{cases} \dot{x}_1(t) = \frac{1}{L} V_{in}(t) \\ \dot{x}_2(t) = -\frac{1}{RC} x_2(t) \end{cases} \tag{II.17}$$

The output equation is:

$$y(t) = i_L(t) \tag{II.18}$$

The state-space representation for this subinterval is:

$$\begin{cases} \dot{x}(t) = A_1 x(t) + B_1 V_{in} \\ y(t) = C_1 x(t) \end{cases} \quad (II.19)$$

Where:

$$A_1 = \begin{bmatrix} 0 & 0 \\ 0 & -\frac{1}{RC} \end{bmatrix} \quad B_1 = \begin{bmatrix} \frac{1}{L} \\ 0 \end{bmatrix} \quad C_1 = [1 \quad 0]$$

B. *Open switch:* On the interval $dT \le t \le T$

The switch ($S_1 = 0$) is open, the diode D_1 conducts, and the equivalent circuit is given in the following diagram Figure II.3 [11], [17].

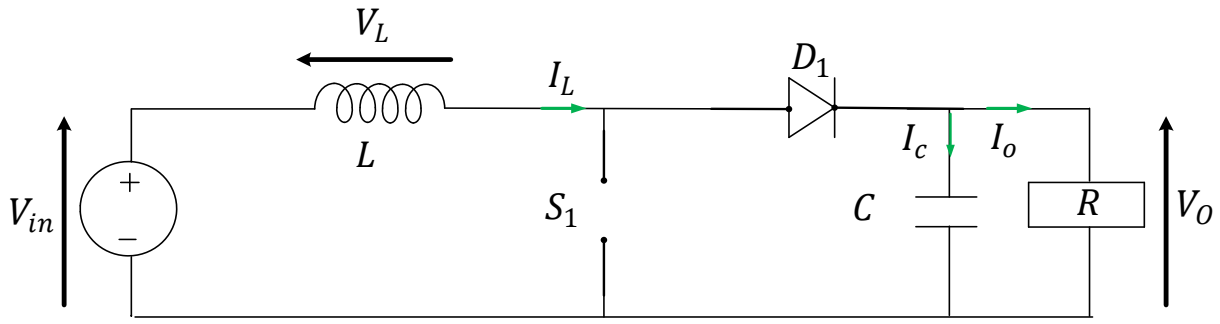

Figure II.3 Boost switch is open

Kirchhoff's Voltage Law around the loop containing L, D_1, C, and R:

$$V_{in} - V_L - V_o = 0 \quad (II.20)$$

Thus:

$$\frac{di_L(t)}{dt} = \frac{V_{in}}{L} - \frac{V_o}{L} \quad (II.21)$$

Using Kirchhoff's law at the output node:

$$i_L(t) = i_C(t) + i_o(t) \quad (II.22)$$

Thus:

$$C\frac{dV_C}{dt} = i_L - \frac{V_o}{R} \quad (II.23)$$

The differential equations for the second mode are:

$$\begin{cases} \dot{x}_1(t) = -\dfrac{1}{L}x_2(t) + \dfrac{1}{L}V_{in}(t) \\ \dot{x}_2(t) = \dfrac{1}{C}x_1(t) - \dfrac{1}{RC}x_2(t) \end{cases} \quad (II.24)$$

The output equation is:

$$y(t) = x_1(t) = i_L(t) \quad (II.25)$$

The state-space representation for this subinterval is:

$$\begin{cases} \dot{x}(t) = A_2x(t) + B_2V_{in} \\ y(t) = C_2x(t) \end{cases} \quad (II.26)$$

Where:

$$A_2 = \begin{pmatrix} 0 & -\dfrac{1}{L} \\ \dfrac{1}{C} & -\dfrac{1}{RC} \end{pmatrix}, \quad B_2 = \begin{pmatrix} \dfrac{1}{L} \\ 0 \end{pmatrix}, \quad C_2 = [1 \quad 0] \quad (II.27)$$

C. State-Space Averaging

To combine the two state-space models (A_1, B_1) for $[0, t_1]$ and (A_2, B_2) for $[t_1, T]$ in (II.19) and(II.26), we use the State-Space Averaging method :

$$\begin{cases} \dot{x} = [A_1D + A_2(1-D)]x + [B_1D + B_2(1-D)]V_{in} \\ y = [C_1D + C_2(1-D)]x \end{cases} \quad (II.28)$$

Thus, the averaged state-space representation of the Boost converter is:

$$\begin{cases} \begin{pmatrix} \dot{x}_1(t) \\ \dot{x}_2(t) \end{pmatrix} = \begin{pmatrix} 0 & -\dfrac{(1-D)}{L} \\ \dfrac{(1-D)}{C} & -\dfrac{1}{RC} \end{pmatrix} \begin{pmatrix} x_1(t) \\ x_2(t) \end{pmatrix} + \begin{pmatrix} \dfrac{1}{L} \\ 0 \end{pmatrix} V_{in} \\ y(t) = [1 \quad 0] \begin{pmatrix} x_1(t) \\ x_2(t) \end{pmatrix} \end{cases} \quad (II.29)$$

II.2.2 Steady-State Analysis and Sizing of Passive Components (L and C)

The design and selection of the boost converter's passive components, namely the inductor (L) and capacitor (C), are predicated on a steady-state analysis. This section outlines the derivation of the analytical expressions required to size these components, with the objective of maintaining the inductor current ripple and output voltage ripple within specified tolerances to guarantee stable converter operation.

II.2.2.1 Inductor Sizing and Current Ripple

Frome the section (II.2.1), when the switch S_1 is on, the voltage across the inductor is:

$$V_L = L\frac{di}{dt} \tag{II.30}$$

The waveform of the inductor current is presented in Figure II.4.

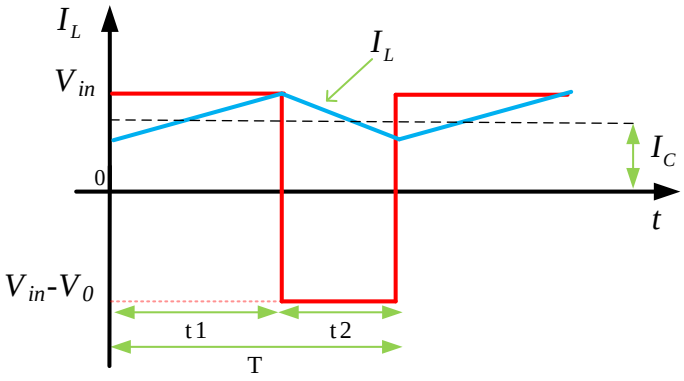

Figure II.4 The Inductor Current

The peak-to-peak ripple current in the inductor is given by:

$$\Delta I_L = \frac{V_{in}}{L}t_1 \tag{II.31}$$

Where $t_1 = D.T$, with D being the duty cycle and T the switching period.

During the interval t_1 (switch closed):

$$V_L = V_{in} = L\frac{\Delta I_L}{t_1} \Rightarrow t_1 = \frac{\Delta I_L L}{V_{in}} \tag{II.32}$$

During the interval t_2 (switch open):

$$V_L = V_{in} - V_o = -L\frac{\Delta I_L}{t_2} \Rightarrow t_2 = \frac{\Delta I_L}{V_o - V_{in}}L \tag{II.33}$$

Where $(\Delta I_L = I_{max} - I_{min})$ is the peak-to-peak ripple current of the inductor L.

From equations (II.32) and (II.33) (assuming volt-second balance on inductor for steady-state) [11]:

$$DI_L = \frac{V_{in}t_1}{L} = \frac{(V_o - V_{in})t_2}{L} \tag{II.34}$$

Substituting $(t_1 = DT)$ *and* $(t_2 = (1 - D)T)$, the average output voltage is:

$$V_o = \frac{V_{in}}{1 - D} \tag{II.35}$$

If the Boost converter is assumed to be lossless ($P_{in} = P_{out}$) [11]:

$$V_{in} I_{in} = V_o I_o \Rightarrow I_{in} = \frac{I_o}{1 - D} \tag{II.36}$$

$$I_{in} = \frac{I_o}{1 - D} \tag{II.37}$$

The switching period T is given by:

$$T = \frac{1}{f} = t_1 + t_2 = L\frac{\Delta I_L}{V_{in}} + L\frac{\Delta I_L}{V_o - V_{in}} = \frac{\Delta I_L L V_o}{V_{in}(V_o - V_{in})} \tag{II.38}$$

From equation (II.38), the peak-to-peak ripple current is:

$$\Delta I_L = \frac{V_{in}(V_o - V_{in})}{f L V_o} \Rightarrow \Delta I_L = \frac{V_{in} D}{f L} \tag{II.39}$$

The inductor current is an internal variable, unlike the output voltage or input current, allowing us to choose (ΔI_L) arbitrarily, for example, 20% of its average value.

The input-output relationship of the converter is from (II.35):

$$V_{in} = V_o(1 - D) \tag{II.40}$$

Substituting (II.40) into the peak-to-peak ripple current:

$$\Delta I_L = \frac{V_o(1 - D)D}{f \cdot L} \tag{II.41}$$

From equation (II.41) the inductance L is:

$$L = \frac{V_o D(1 - D)T_s}{\Delta I_L} \tag{II.42}$$

To locate the worst case, we differentiate L(D) with respect to the duty ratio D:

$$\frac{dL(D)}{dD} = \frac{V_o T_s}{\Delta I_L}(1 - 2D) = 0 \tag{II.43}$$

From (II.43) the "worst-case" for ripple (largest ripple for a given L, or largest L needed for a given ripple constraint) is often considered at D=0.5.

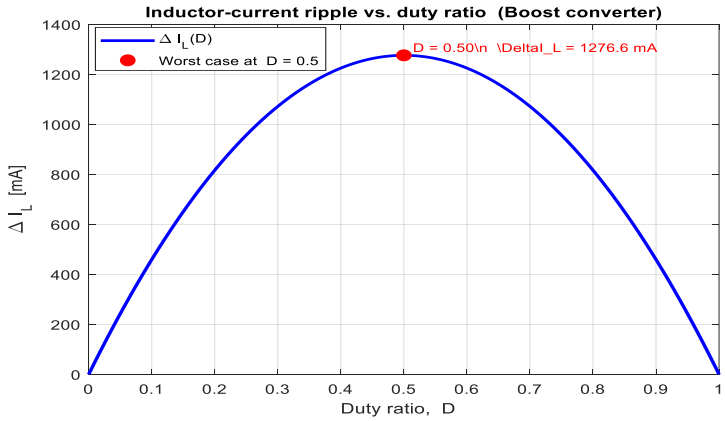

Figure II.5 Inductor-current ripple vs. duty ratio (Boost converter)

The inductor-current ripple ΔI_L versus duty ratio follows a concave (parabolic) profile:

- Horizontal axis: duty cycle D ($0 \rightarrow 1$)
- Vertical axis: ΔI_L
- Peak ripple occurs at D=0.5 with

$$\Delta I_{L,\max} = \frac{V_o T_s}{4L} \qquad (II.44)$$

Hence, sizing the inductance at—or near—D=0.5 guarantees acceptable ripple for every other value of D in the converter's operating window.

II.2.2.2 Capacitor Sizing and Output Voltage Ripple

When the switch S_1 is closed, the capacitor supplies the load current during $t = t_1$. The average capacitor current in this case is I_o (Figure II.6) [11].

$$\Delta V_C = \frac{1}{C}\int_0^{t_1} I_o\,dt = \frac{I_o t_1}{C} \qquad (II.45)$$

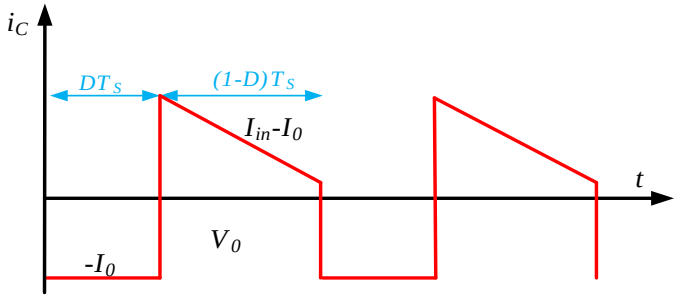

Figure II.6 The capacitor current waveform in a Boost Converter

Substituting ($t_1 = DT_S = D/f$):

$$\Delta V_o = \frac{I_o D}{fC} \quad (II.46)$$

From equation (II.46):

$$\Delta V_o = \frac{I_o D}{fC} \Rightarrow C_{min} = \frac{I_o D}{f \Delta V_o} \quad (II.47)$$

II.2.2.3 Application

To interface a photovoltaic (PV) source with a DC load, a Boost converter is designed to match the power and voltage levels required. The design is based on the maximum power point (MPP) of the PV module and aims to ensure high efficiency through proper sizing of the passive components.

PV Source Specifications

The PV system operates under standard irradiance conditions with a solar irradiance G=1000 W/m². The electrical parameters of the PV module at the maximum power point (MPP) are:

- $I_{mp} = 9.58A$; $V_{mp} = 33.4V$; $P_{mp} = 319.17W$
- The output voltage: $V_o = 74V$.
- Assuming a converter efficiency of 90%, the power delivered to the load is:

$$P_{load} = 0.9 \cdot P_{mp} = 287.25W \quad (II.48)$$

- Based on the principle of energy conservation and the steady-state voltage relation for the Boost converter, the duty cycle D is estimated as:

$$D = 1 - \frac{V_{in}}{V_0} = 1 - \frac{33.4}{74} \approx 0.54 \quad (II.49)$$

- The maximum output current is then calculated as:

$$I_{Lmax} = V_0 / P_{load} = 3.88A \quad (II.50)$$

- From this, the equivalent load resistance is estimated:

$$R = V_0 / I_{Lmax} \approx 15\Omega \quad (II.51)$$

- The switching frequency:

$$f_s = 33kHz \quad (II.52)$$

Inductor Sizing

On this design of inductor, we assume that the ripple current $\Delta I_L = 20\%$ of I_L

The inductance can be calculated by equation (II.44):

$$L_{\min} = \frac{V_o}{4 f_s \Delta I_{L.\max}} = \frac{74}{4 \times 33 \times 10^3 \times 0.2} = 0.720 mH \qquad (II.53)$$

Output Capacitor Sizing

To ensure stable voltage regulation, a small output voltage ripple is allowed, defined as:

ΔV_o=10% of V_0

output capacitor can be calculated by equation (II.47):

$$C_{min} = \frac{I_o D}{f \Delta V_o} = 0.11 mF \qquad (II.54)$$

II.2.3 PV array dynamic performance evaluation

II.2.3.1 Open loop response of PV array with Boost dc-dc converter

The open-loop response of the PV array coupled to a boost DC-DC converter was tested under dynamic environmental conditions (Figure II.7).

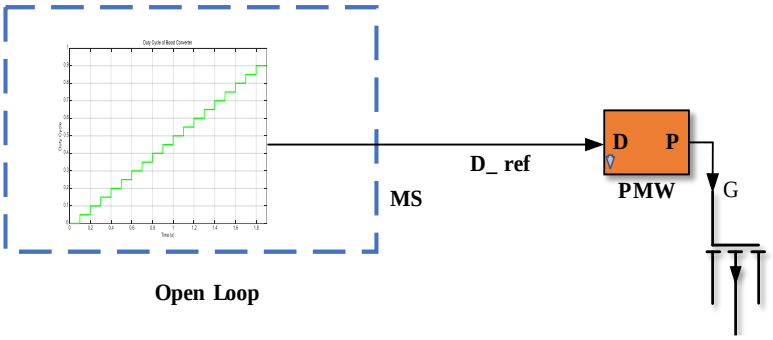

Figure II.7 Association PV array/boost DC-DC Boost converter (Open Loop) [13].

A predefined duty cycle sweep (Figure II.8) was applied to the converter switch. System outputs (voltage, current, power) were recorded under:

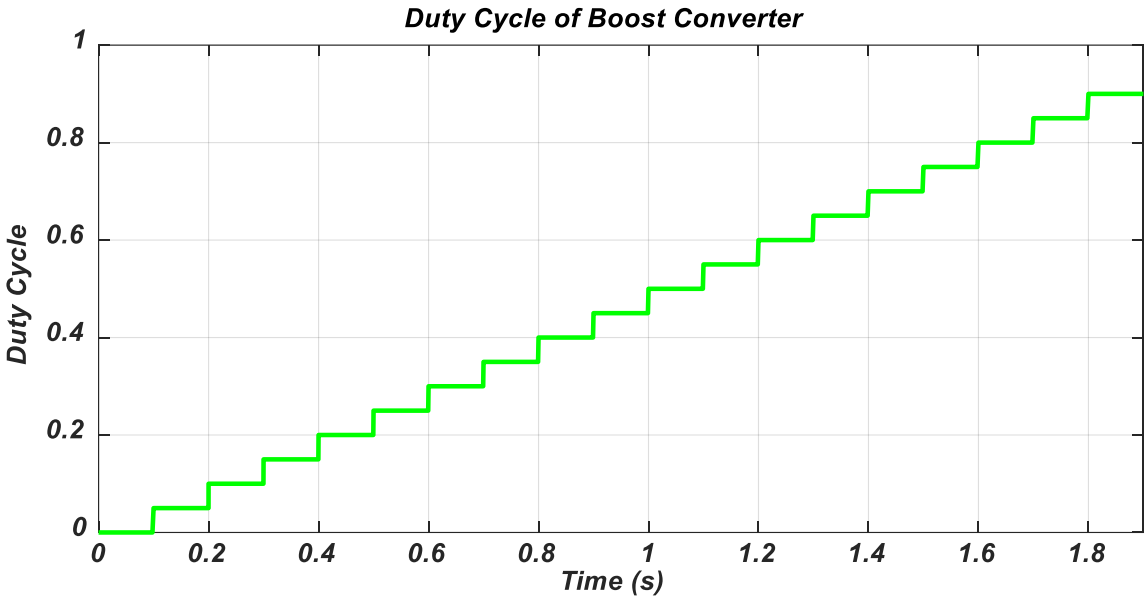

Figure II.8 Duty cycle evolution used to drive the open loop response of the association PV array/boost DC-DC converter.

to simplify the task and be more objective, we have exploited the Sim Power Systems TM library models of Matlab software. Table B illustrates the simulation parameters in our case study.

Table B Simulation parameters

Sample time; T_S	discrete: 2e-6 s
Control time , T_C	2e-5 s
Output capacitor, C_{dC}	47 µF
Input capacitor, C_{PV}	2000 µF
Inductor, L_{PV}	0.7 mH
Switching frequency, fs	33 KHz

As it can be noted in the open loop responses of the PV generation system, the open loop response in the case of a change in temperature or irradiation in Figure II.9 and Figure II.10 have minor changes on the responses in each operating region.

Open-loop operation exhibits instability under environmental shifts. Voltage/power deviations exceed 50%, validating the need for closed-loop MPPT control.

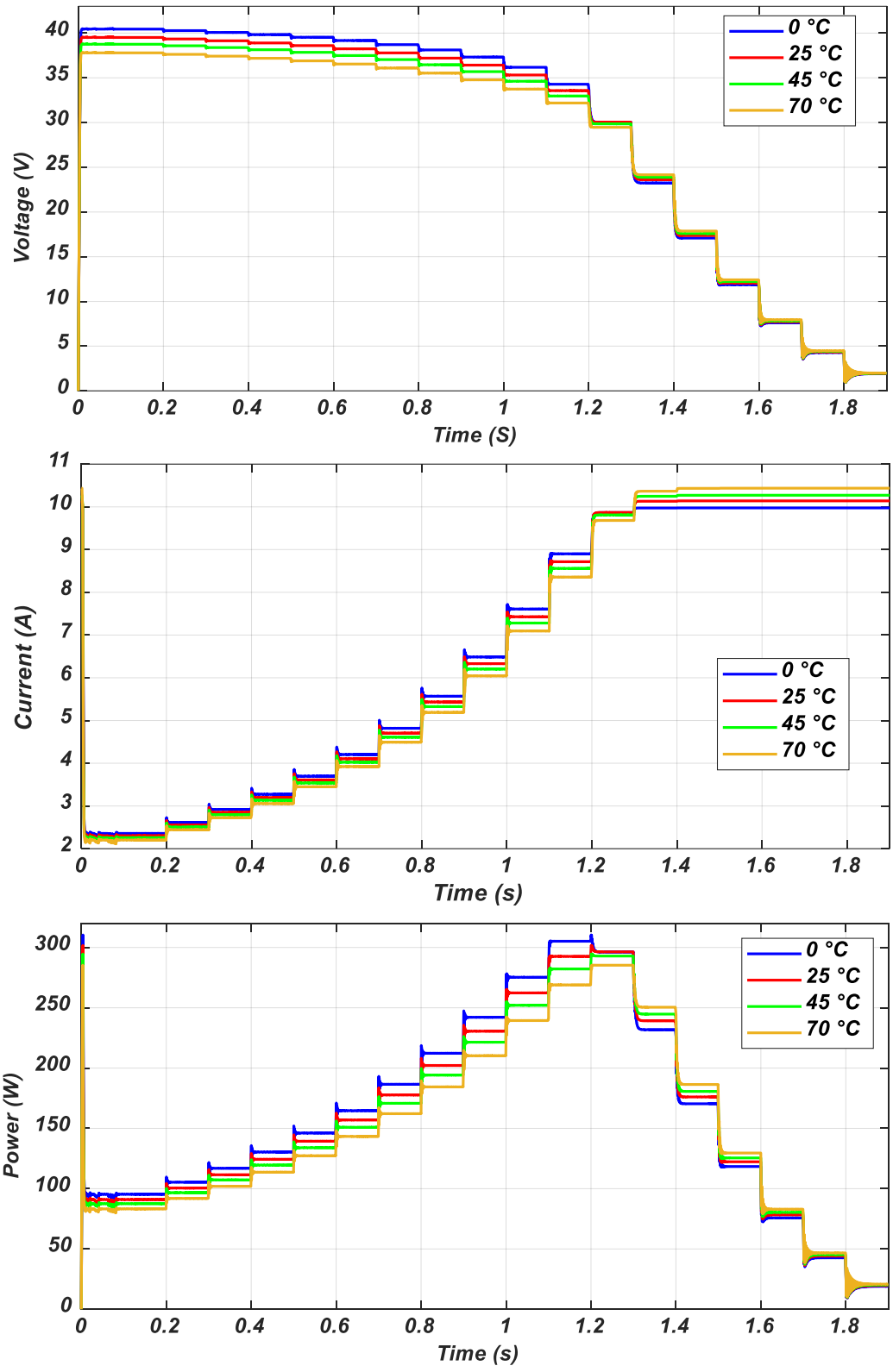

Figure II.9 Open loop response to variation of temperature.

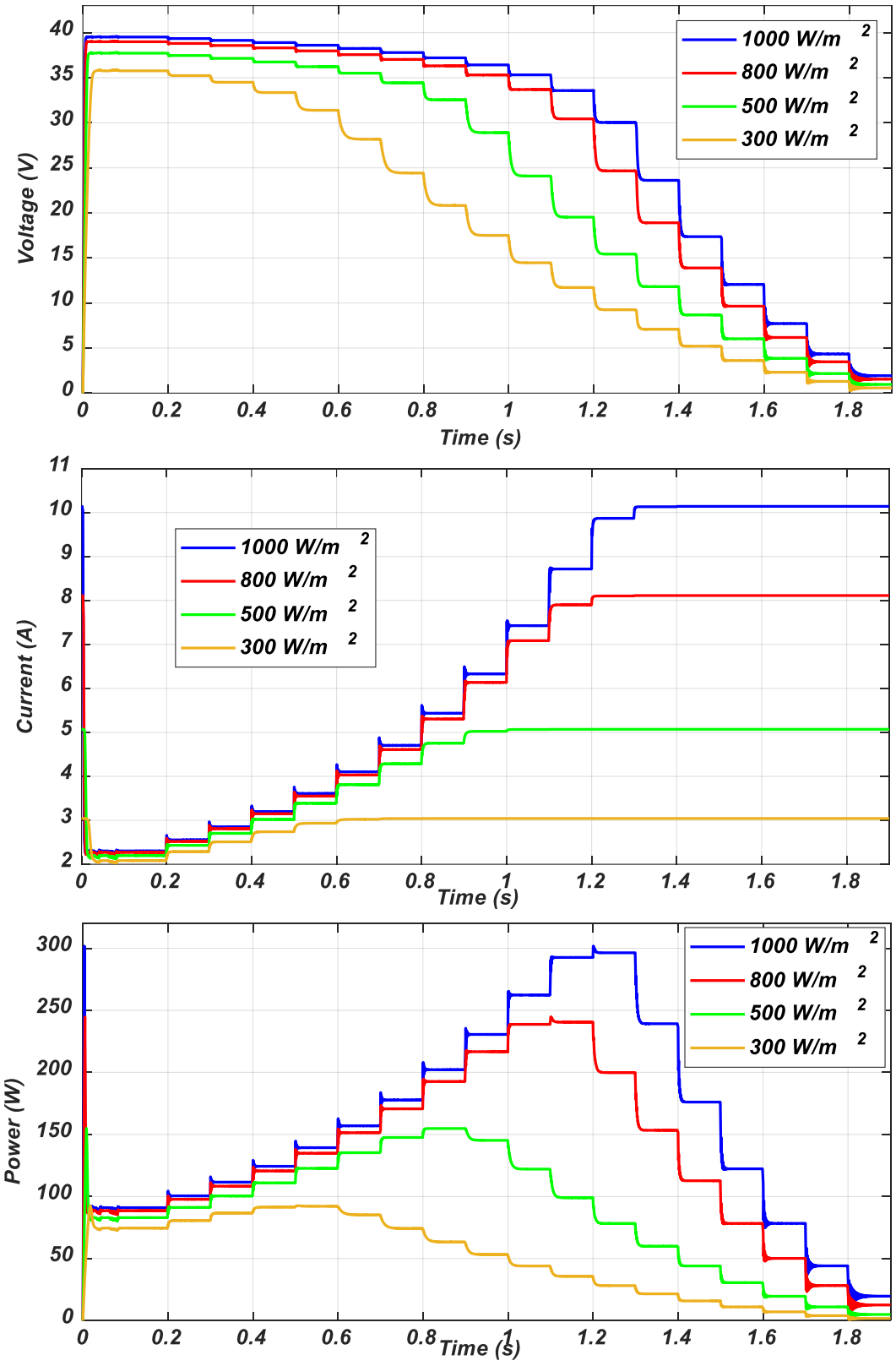

Figure II.10 Open loop response to variation of irradiation.

II.2.4 MPPT perturb and observe PO

The PO algorithm tracks the Maximum Power Point (MPP) by perturbing the operating point and observing power changes. To evaluate its dynamic performance, the system was subjected to a sudden load change by modifying the load resistance R at t=2s. Two common implementations of the PO algorithm are evaluated and compared: a direct method and an PO control method.

II.2.4.1 Direct PO MPPT method

Method: The duty cycle (D) of the boost converter is perturbed directly by the PO algorithm to track the MPP. The system's response to a load disturbance is observed to assess its tracking effectiveness and stability.

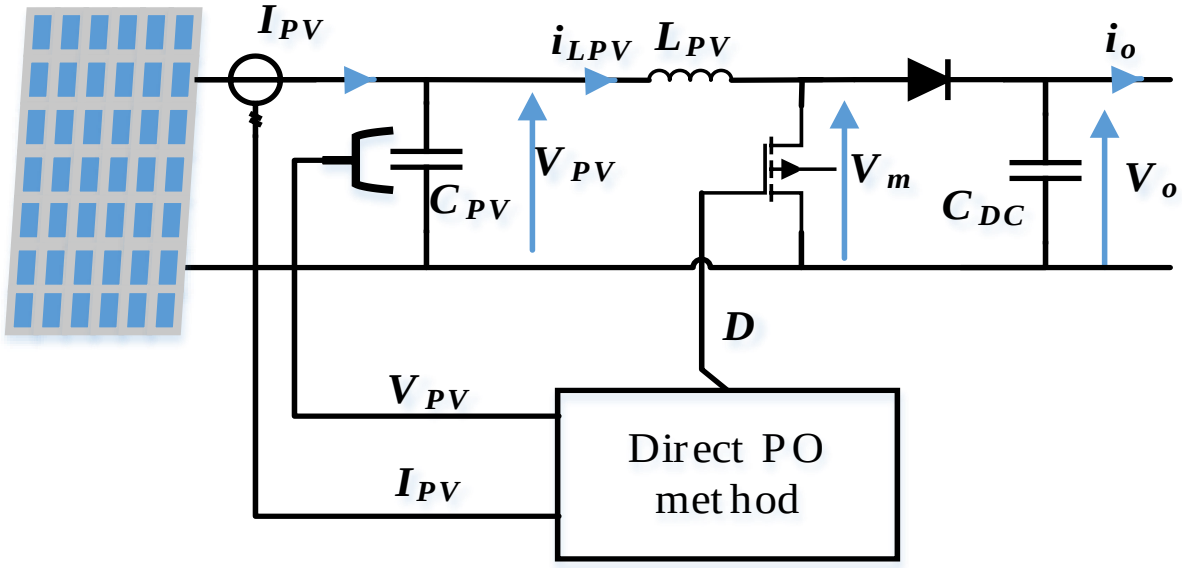

Figure II.11 Schematic Diagram of Photovoltaic System with DC-DC Boost Converter and Direct PO MPPT Control.

Simulation results and discussion

The simulation results in Figure II.12 demonstrate the effectiveness of the direct Perturb and Observe (P&O) MPPT algorithm in maintaining the maximum power point (MPP) despite variations in the load.

- At the beginning of the simulation, the load is fixed (R=20 Ohms), and the MPPT algorithm quickly adjusts the duty cycle (Figure II.12a) to reach the maximum power point corresponding to the environmental conditions (irradiance of 1000 W/m² and temperature of 25°C). This leads to a stable operating point with maximum power extraction.
- Figure II.12b shows the PV current evolution. Once the MPP is reached, the PV current stabilizes, indicating that the operating point is well regulated.
- Figure II.12c presents both the PV voltage and the load voltage. Initially, both voltages stabilize when the MPP is achieved. However, when the load is changed (R=40 Ohms), the load voltage varies in response to the new load impedance, while the PV voltage remains nearly constant, proving that the MPPT algorithm continues to maintain the panel at the maximum power point.
- Figure II.12d illustrates the PV power. It remains stable at its maximum value even after the load changes, confirming that the direct P&O method effectively decouples the source

optimization from the load behavior. The power delivered by the PV array remains optimal, despite the variation in load.

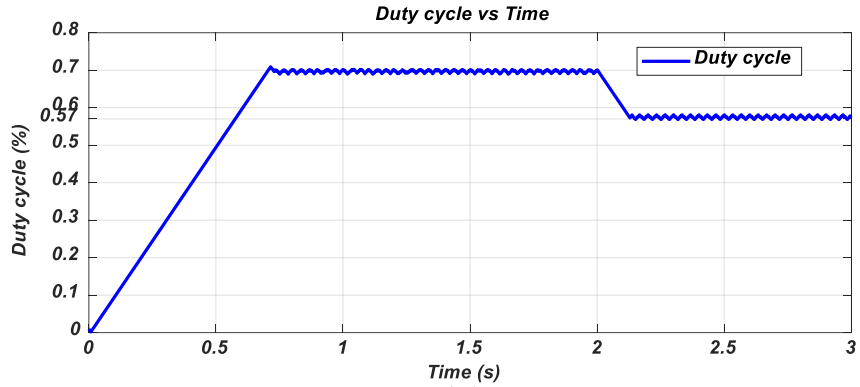

(a)

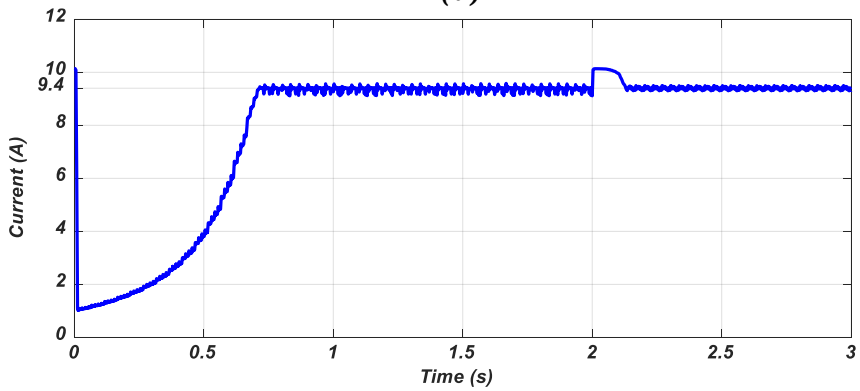

(b)

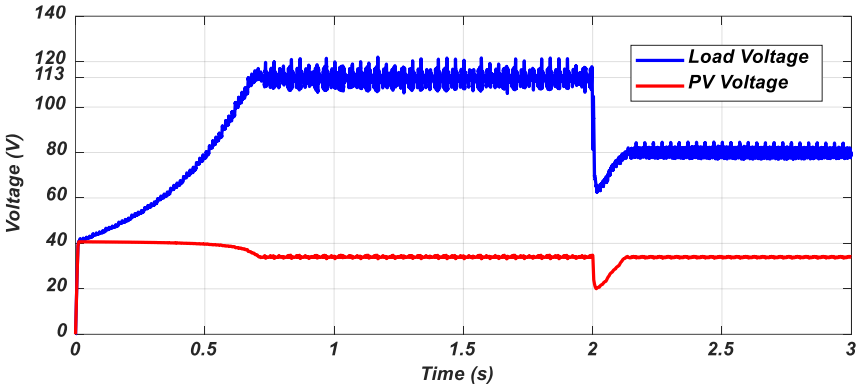

(c)

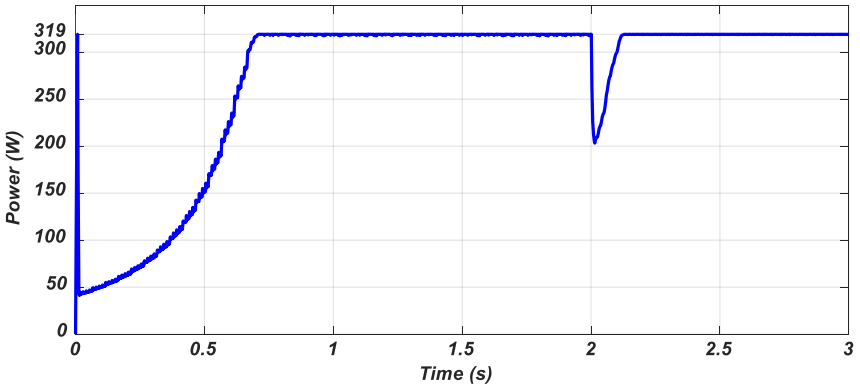

(d)

Figure II.12 Tracking of the MPP with change of load (in MATLAB) by direct PO of a) Duty cycle, b) PV Current c) PV and Load Voltages and d) PV Power

A. Control of MPPT method

Control of MPPT method PO method uses cascaded control where the MPPT algorithm perturbs the voltage reference ($V_{PV,ref}$) instead of directly controlling the duty cycle. Two PI controllers work in tandem: a slow outer voltage loop (PI_V) that converts voltage error into current reference, and a fast inner current loop (PI_I) that modulates the duty cycle to track this current reference.

This two-speed architecture separates slow MPPT dynamics from fast converter control, enabling superior disturbance rejection and transient response. The PV current acts as an external disturbance to the voltage loop, while the duty cycle emerges indirectly through the current control pathway.

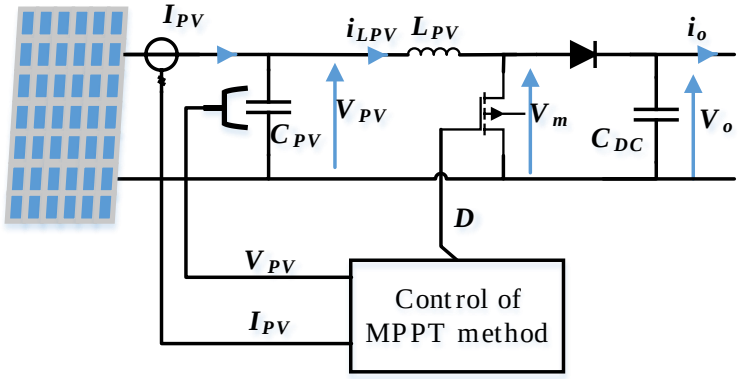

Figure II.13 Schematic Diagram of Photovoltaic System with DC-DC Boost Converter and PO MPPT Control.

As shown Figure II.14, when the reference voltage comes from the PV algorithm (MPPT algorithm), the output of the first controller provides the reference current required to charge or discharge the capacitor to the desired voltage. This reference current is then fed to the second PI_I controller, whose output generates the reference for the average voltage applied across the inductor. By applying Kirchhoff's laws, the modulated PV voltage reference is obtained, which depends on the DC voltage and the duty cycle of the PV converter.

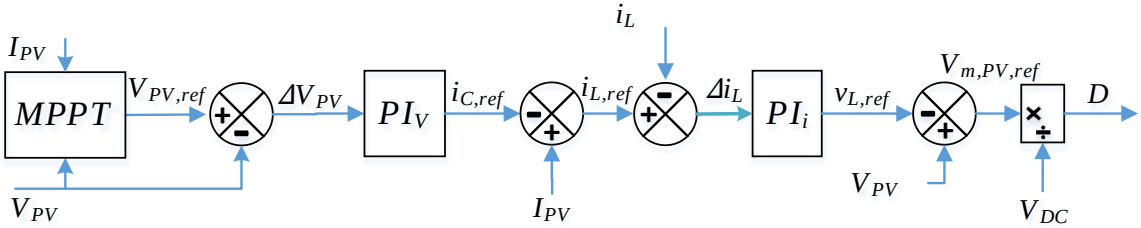

Figure II.14 Block Diagram of Photovoltaic MPPT Control System Employing Cascaded PI Controllers.

Control Law Using a PI Controller

We consider the photovoltaic current (I_{PV}) from the photovoltaic generator as a disturbance signal, and the power converter (Boost) as two linear subsystems, with certain disturbance signals (Figure II.15).

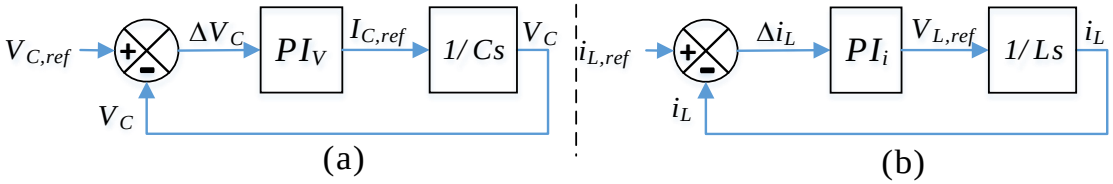

Figure II.15 Linearized Models of Control Subsystems for Voltage and Current Regulation in DC-DC Converters.

The mathematical model of the first subsystem is given by:

$$\frac{d}{dt}V_{PV} = \frac{1}{C_{PV}}I_{C_{PV}} \tag{II.55}$$

$$\frac{d}{dt}i_{L,PV} = \frac{1}{L_{PV}}V_{L,PV} \tag{II.56}$$

From Figure II.14, we can derive the following equations:

$$i_C = I_{PV} - i_{L,PV} \tag{II.57}$$

$$V_{m,PV} = V_{PV} - V_{L,PV} \tag{II.58}$$

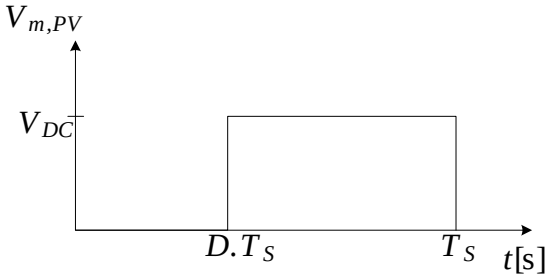

Figure II.16 Waveform of Modulated PV Voltage

Figure II.16 illustrates the waveform of the modulated PV voltage and presents equation:

$$\bar{V}_{m,PV} = V_{m,PV,ref} = V_{DC}(1 - D) \tag{II.59}$$

Thus:

$$D = 1 - \frac{\bar{V}_{m,PV}}{V_{DC}} \tag{II.60}$$

Simulation results and discussion

The presented results illustrate the performance of an Perturb and Observe (P&O) MPPT control strategy applied to a photovoltaic (PV) system using a Boost converter. This method differs from the direct approach by generating a reference voltage corresponding to the maximum power point (MPP), which is then regulated through two cascaded control loops:

1. An outer loop to regulate the PV voltage toward the reference voltage generated by the MPPT algorithm.
2. An inner loop to regulate the inductor current, ensuring accurate and stable duty cycle control.

- At the beginning of the simulation, the load is fixed. The MPPT algorithm identifies the optimal operating point under standard test conditions (irradiance of 1000 W/m² and temperature of 25°C), and provides the corresponding reference voltage. The voltage control loop adjusts the PV voltage to track this reference, and the current control loop ensures smooth converter operation. As seen in the figures, the regulation is effective, and the PV system quickly reaches the MPP. The PV power remains constant and equal to the maximum value, indicating that the cascaded control system (MPPT + voltage + current control) effectively maintains optimal operation.
- When the load changes, the output voltage of the Boost converter varies, reflecting the new load impedance. However, the PV voltage remains constant, controlled to match the MPPT reference. As a result, the power extracted from the PV array remains unchanged, highlighting the robustness of this control strategy against load variations.
- Overall, the simulation results confirm that this control of MPPT method approach successfully decouples the source optimization from load dynamics, ensuring maximum power extraction under varying load conditions.

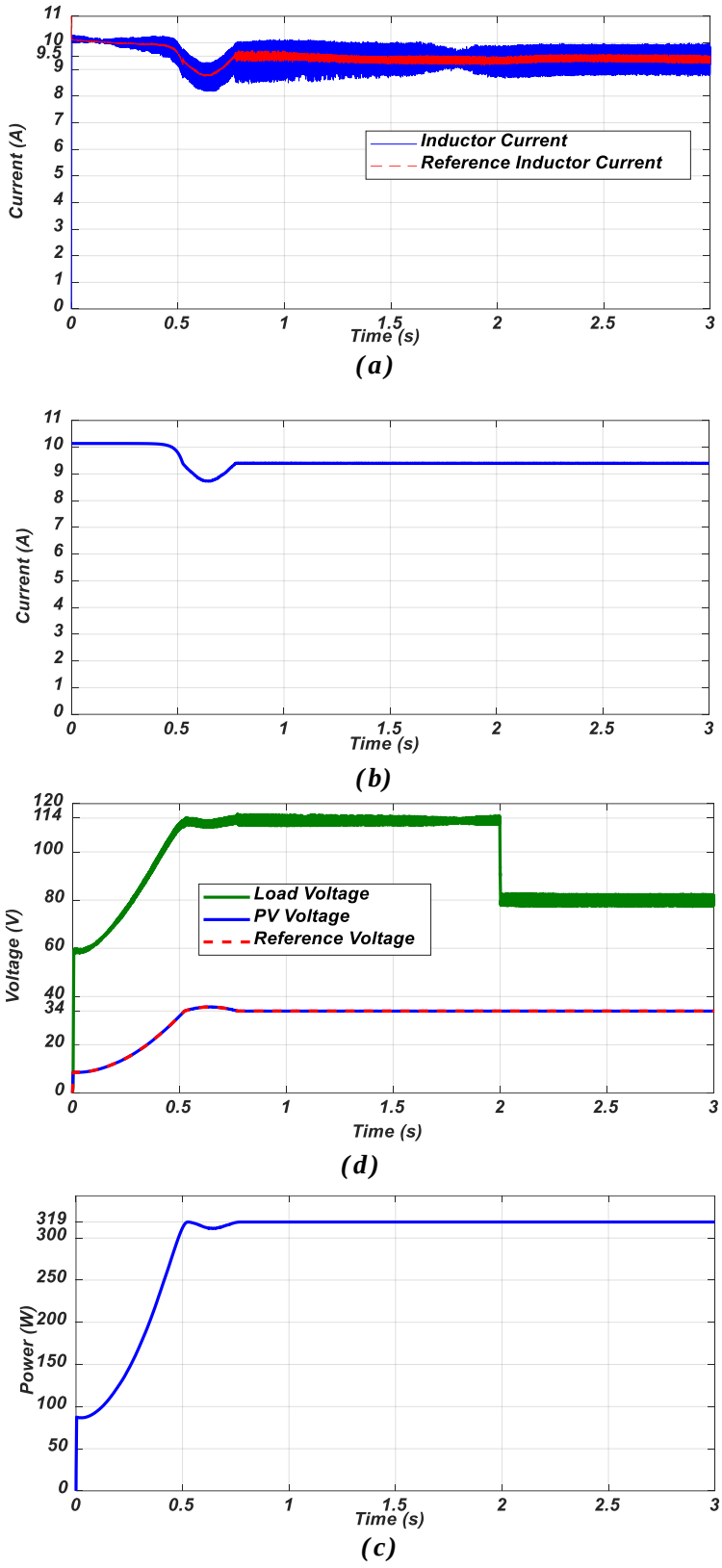

Figure II.17 Tracking of the MPP with change of load (in MATLAB) by control of MPPT method (PO) of a) Inductor and Reference Inductor Currents, b) PV Current c) Load, PV and Reference PV Voltages and d) PV Power

II.3 Conclusion:

This chapter successfully established the theoretical and simulated framework for a boost converter-based PV MPPT system. Beginning with a detailed mathematical analysis, the chapter derived the state-space models for the converter's distinct operating states (switch ON and switch OFF). Through the application of state-space averaging, these were consolidated into a single, comprehensive model that accurately represents the converter's dynamic behavior. This foundational analysis was then extended to practical design considerations, yielding the essential equations for sizing the inductor (L) and capacitor (C) to effectively constrain current and voltage ripple, with a key finding that the worst-case inductor ripple occurs at a duty cycle of $D=0.5$.

The open-loop simulations performed were critical in demonstrating the PV system's inherent sensitivity and instability when subjected to varying environmental conditions. The results clearly showed that both voltage and power outputs fluctuate significantly with changes in temperature and irradiation, underscoring the indispensable need for a robust, closed-loop control system to maintain optimal performance.

The core contribution of this chapter was the comparative evaluation of two Perturb and Observe (PO) MPPT implementations under a sudden load disturbance. The direct PO method, while successful in tracking the MPP, exhibited a significant transient dip in power and voltage, highlighting a potential weakness in applications requiring high stability. In stark contrast, the control of MPPT method PO, architected with a cascaded PI control structure, demonstrated vastly superior dynamic performance. Its ability to reject the load disturbance with minimal deviation in PV power and voltage confirmed its robustness and efficiency.

In summary, this chapter has not only modeled the power electronic interface but has also, through simulation, validated the functional superiority of the cascaded control architecture for MPPT applications. Having established a reliable model and a promising control strategy, the stage is now set for the crucial next step: the transition from simulation to practice. The following chapter will focus on the experimental validation of these control schemes using a dSPACE platform to verify their real-world performance.

Chapter III

Experimental Validation OF MPPT Control Using dSPACE

III. Experimental Validation OF MPPT Control Using dSPACE

III.1 Introduction

Building upon the theoretical foundations of photovoltaic systems established in Chapter 1 and the detailed analysis of DC-DC converters along with their preliminary MPPT simulations in Chapter 2, this chapter transitions directly to the critical stage of practical experimental validation. The primary focus is to rigorously evaluate the performance of Maximum Power Point Tracking (MPPT) control strategies through their real-time implementation and testing using a dSPACE. This chapter aims to bridge the gap between the preceding analytical work and tangible, real-world performance assessment.

The core of this chapter details the experimental validation using the dSPACE DS1104 platform. The discussion will commence with an overview of the dSPACE system and the specific experimental setup configured for these tests, highlighting the use of the dSPACE Control Desk software for real-time monitoring, parameter adjustment, and the crucial task of data acquisition for subsequent analysis and figure generation. This is followed by the vital step of characterizing a real photovoltaic module under actual operating conditions to establish a baseline, and conducting open-loop system tests to understand its inherent dynamic response. The culmination of this chapter is the deployment and thorough testing of selected MPPT algorithms, such as direct and control MPPT methods, on the dSPACE controller. The results obtained from these experiments, visualized and recorded via Control Desk, will be meticulously analyzed to assess the tracking efficiency, dynamic response, and overall robustness of the MPPT controllers in a near-real-world environment, thereby validating the efficacy of the developed control schemes.

III.2 Overview of the dSPACE DS1104 R&D Controller Board

The DS1104 is a powerful control board developed by dSPACE, specifically designed for rapid control prototyping. Its high processing capability and rich set of input/output interfaces make it particularly suitable for advanced control applications that involve multiple actuators and sensors. Programmable within the Matlab/Simulink environment [18], the DS1104 facilitates seamless implementation and testing of complex control algorithms. The system is composed of two main parts: an interface board equipped with a DSP processor that connects the control panel to the host computer, allowing for real-time data acquisition and processing; and a control panel featuring various connectors such as BNC terminals for analog-digital conversion, PWM outputs, digital I/O ports, RS232/RS422 serial interfaces, and encoder inputs, enabling flexible interaction with external hardware components [18]. It's a quick and easy way to implement control functions, the Figure III-1 shown the card of dSPACE 1104.

Figure III-1 Card of dSPACE 1104

The card has a connection panel that includes I/O devices that allow communication with the physical system. The next figure, illustrates the connection panel of the dSPACE 1104

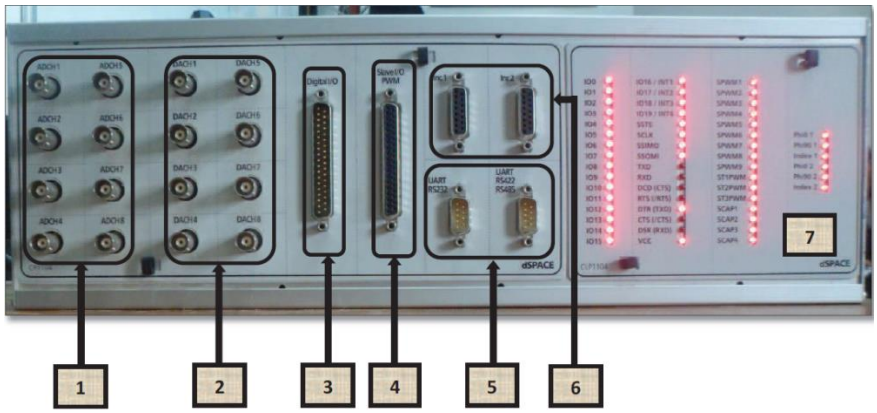

Figure III-2 Connection panel of the dSPACE 1104

(1) ADC digital analog converters
(2) DAC analog digital converters
(3) Digital input / output interface, used for programming languages.
(4) I / O interface of the DSP responsible for the generation of PWM control signals.
(5) Serial ports (RS 232, RS 422 and RS 485) are used to connect the board in series with various electronic devices, such as PLCs or with another DS card.
(6) Two encoders allow communication with the position sensors.
(7) The LED lamps indicating the active input / output on the panel.

III.3 A Practical Dynamic Performance Evaluation of the PV System

Before evaluating the control algorithms, the baseline performance of the SW320M-60 PV module [10] was established using the experimental setup shown in Figure III-3. To understand the module's behavior under varying real-world conditions, its characteristic curves were recorded at three different times, corresponding to different levels of solar irradiance:

- Morning: Wednesday, May 28, 2025, 07:57:48 AM
- Afternoon: Wednesday, May 28, 2025, 3:05:21 PM
- Evening: Tuesday, May 27, 2025, 5:02:19 PM

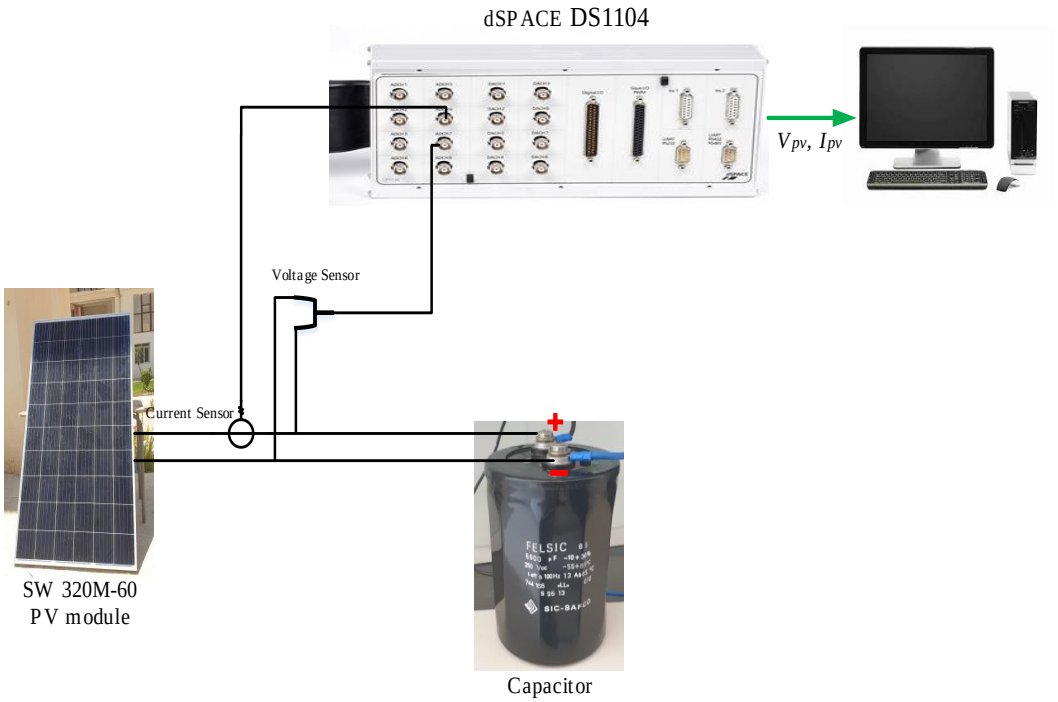

Figure III-3 Schematic of the Experimental Setup for PV Module Characterization

The resulting experimental Current-Voltage (I-V) and Power-Voltage (P-V) curves are presented in Figure III-5 and Figure III-6, respectively.

The comparative I-V curves in Figure III-5 clearly demonstrate that the short-circuit current (I_{sc}) is highly dependent on solar irradiance, decreasing significantly from morning to evening finally to afternoon. In contrast, the open-circuit voltage (V_{oc}) shows a much smaller variation. Consequently, as seen in the P-V curves in Figure III-6, the maximum available power from the module changes drastically throughout the day. These curves validate the non-linear behavior of the module and serve as the practical benchmark for assessing the effectiveness of the MPPT controller under dynamic weather conditions.

Figure III-4 SW320M-60 PV Module

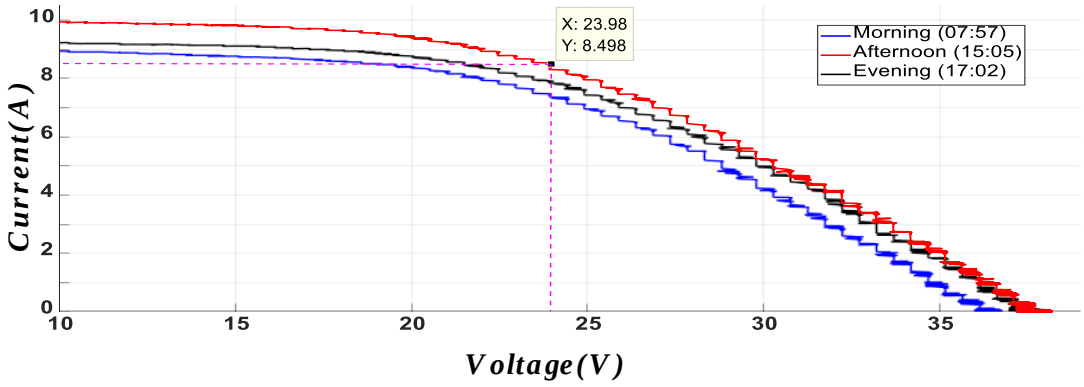

Figure III-5 Comparative I-V Characteristics of the SW320M-60 Module at Different Times of Day.

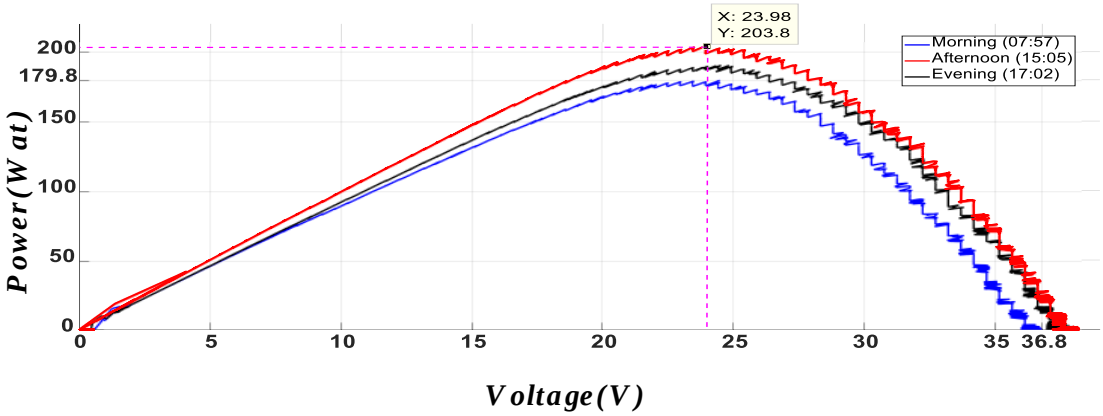

Figure III-6 Comparative P-V Characteristics of the SW320M-60 Module at Different Times of Day.

III.4 Boost Converter Component Details

A critical part of the test bench shown in Figure III-11 is the power stage, which is built around a custom boost converter. The key physical components selected for this converter are detailed below and shown in Figure III-8.

III.4.1 Inductor (L)

Following the design methodology outlined in Chapter 2 (II.42), a target inductance was calculated. To verify the value of the physical component, its inductance was measured experimentally during the t_{ON} and t_{OFF} periods of a switching cycle using an oscilloscope. The resulting current ripple waveform captured for this measurement is shown in Figure III-7. With the system operating at a PV voltage (V_{pv}) of 28.63 V and an output voltage (V_o) of 44.3 V, the following measurements were recorded:

* **During t_{ON} (switch closed):** The current ripple (ΔI_L) was measured as 0.528 A over a time interval (Δt) of 13 µs. The inductance is calculated as:

$$L = \frac{V_{pv}.\Delta t}{\Delta I_L} = \frac{28.63 \times 13}{0.528} \approx 0.70mH \quad (3.61)$$

* **During t_{OFF} (switch open):** The current ripple (ΔI_L) of 0.528 A was measured over a time interval (Δt) of 20 µs. The inductance is calculated as:

$$L = \frac{(V_o - V_{pv}) \times \Delta t}{\Delta I_L} = \frac{(44.3 - 28.63) \times 20}{0.528} \approx 0.59 mH \quad (3.62)$$

The experimental measurement during the t_{ON} period confirms the inductor value of 0.70 mH, aligning with the component selected for the MPPT experiments.

During testing, it was observed that inductor noise could be traced to the physical vibration of the copper windings and the presence of an air gap in the core. Furthermore, care was taken to avoid inductor saturation, a condition identified on the oscilloscope when the inductor current curve begins to bend upwards. An increase in the inductor's air gap was noted to decrease its saturation current (I_{sat}).

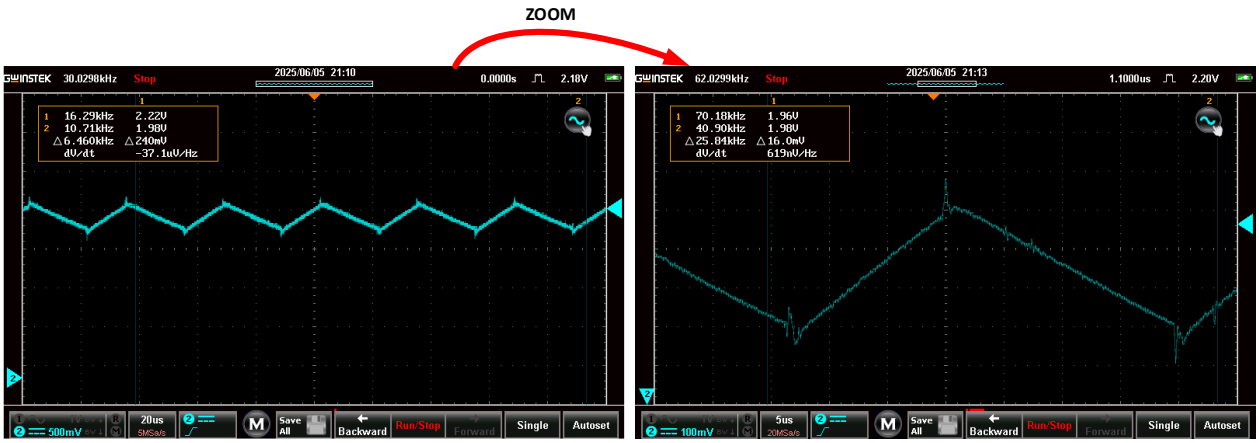

Figure III-7 Oscilloscope Measurement of the Inductor Current Ripple for Inductance Verification.

Figure III-8 Inductor component (0.70 mH)

III.4.2 IGBT Switch

A Toshiba "50JR22" IGBT was selected as the main switching element for the converter due to its suitable voltage and current ratings.

Figure III-9 Toshiba "50JR22" IGBT Switch

To protect the IGBT from voltage spikes inherent in switching converters, snubber circuits are essential. It is also critical to operate within the specified maximum voltage ratings. The selection of the switch must also account for parasitic capacitances that exist between any two of its terminals.

III.4.3 Output Capacitor (C_{dc})

In accordance with the design principles for the output capacitor in Chapter 2 (II.47), a 470µF capacitor was selected to smooth the DC voltage supplied to the load.

Figure III-10 250V 470µF Output Capacitor

III.5 Practical Open loop response

The full experimental test bench, incorporating the SW320M-60 module, boost converter, and the dSPACE control system as detailed in Figure III-11, was first tested in an open loop configuration. To verify the system's dynamic response and to manually identify the Maximum Power Point (MPP), an open-loop test was conducted. The duty cycle (D) of the boost converter was progressively increased from 0 to approximately 0.9 (Figure III-12).

The PC interface designs and compiles the algorithm, which runs on the dSPACE CPU. The Gate Drive (HCPL 3120) requires an external +15V supply and acts as an isolator, stepping up the 5V PWM signal from the dSPACE board to drive the IGBT. The current (LA55TP) and voltage sensors also require a dedicated power supply for operation.

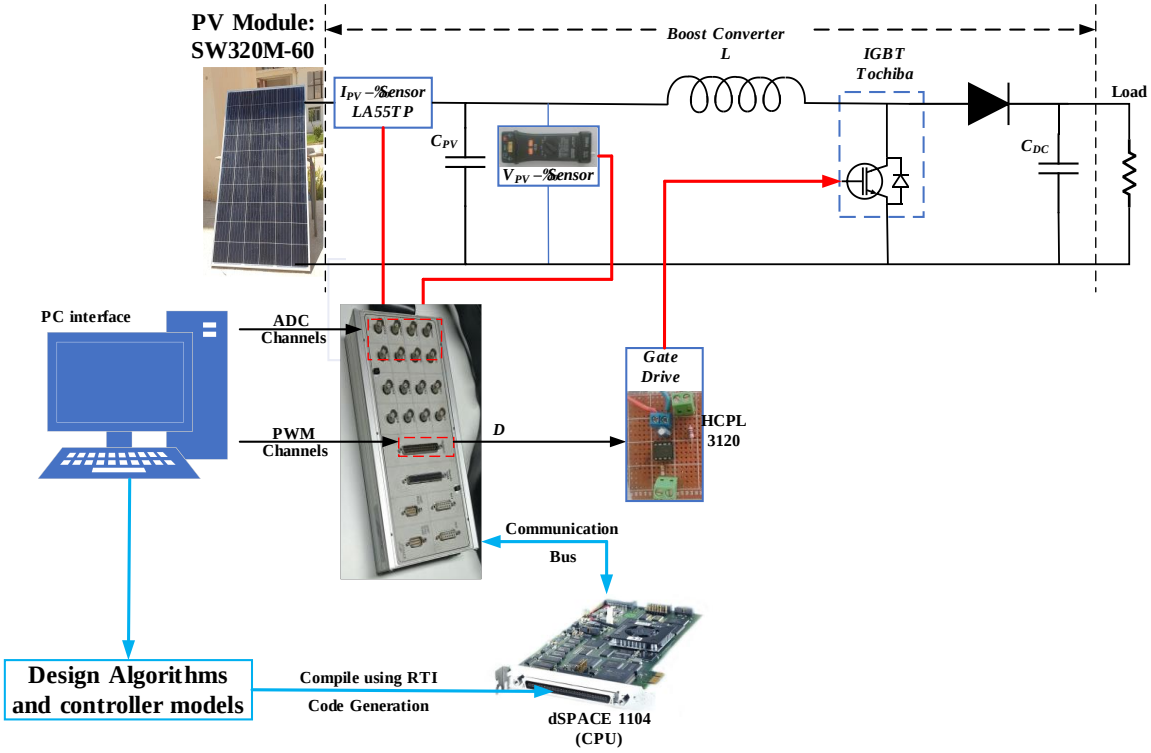

Figure III-11 Detailed Schematic of the Experimental Test Bench for MPPT Control

The open-loop tests highlighted critical operational principles. It was confirmed that a power supply, even one rated for a high current like 10A, will only deliver the current demanded by the load. A key safety consideration when manually controlling the duty cycle is that operating the IGBT at a very low frequency is dangerous. The resulting long on-time (t_{ON}) can allow current to build up beyond the device's maximum rating (I_{max}), leading to component failure. This underscores the importance of the closed-loop controller's role in maintaining safe operating limits.

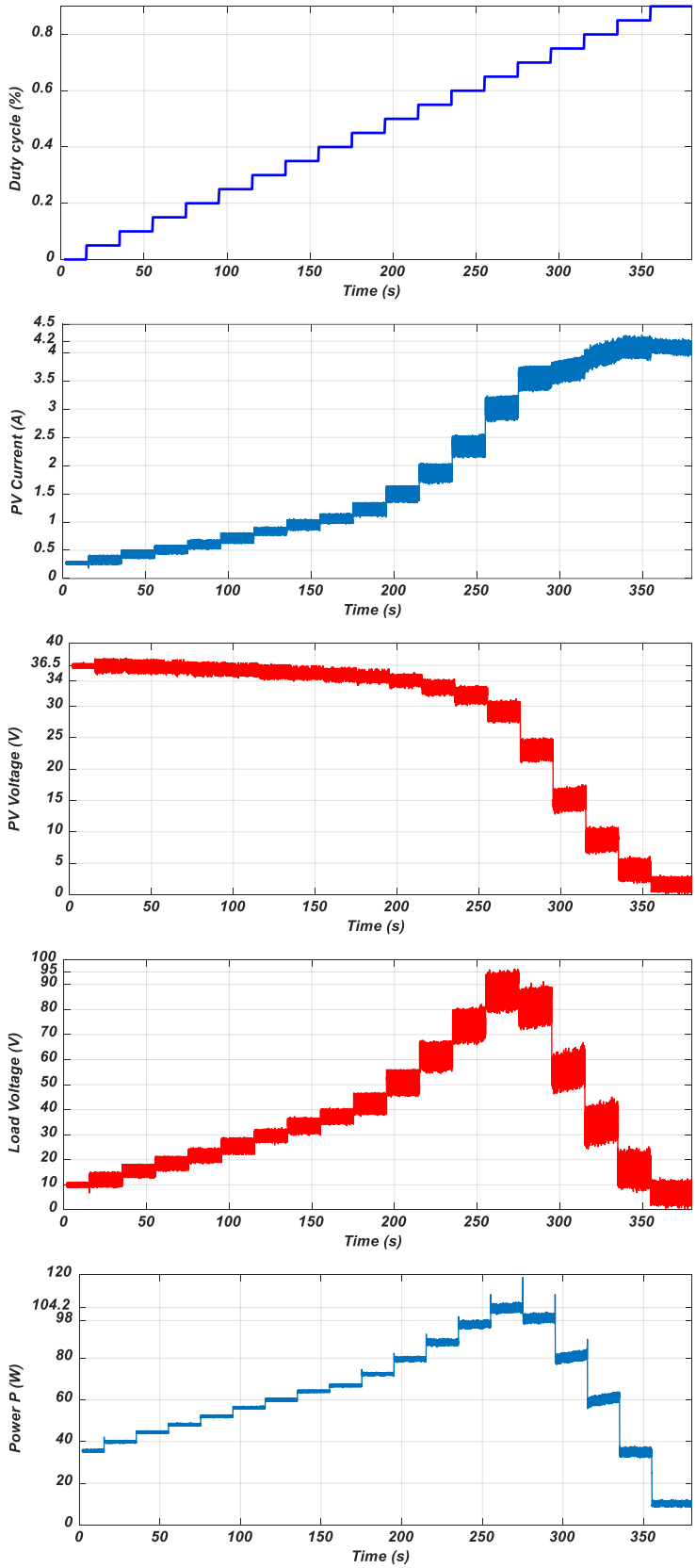

Figure III-12 Experimental open loop response to variation of irradiation to Duty cycle evolution

III.5.1 Experiment Of MPPT Control

Following the open-loop validation, the closed-loop MPPT control algorithms were implemented and tested to evaluate their ability to automatically track the MPP. The following subsections detail the performance of both direct and control of MPPT method strategies.

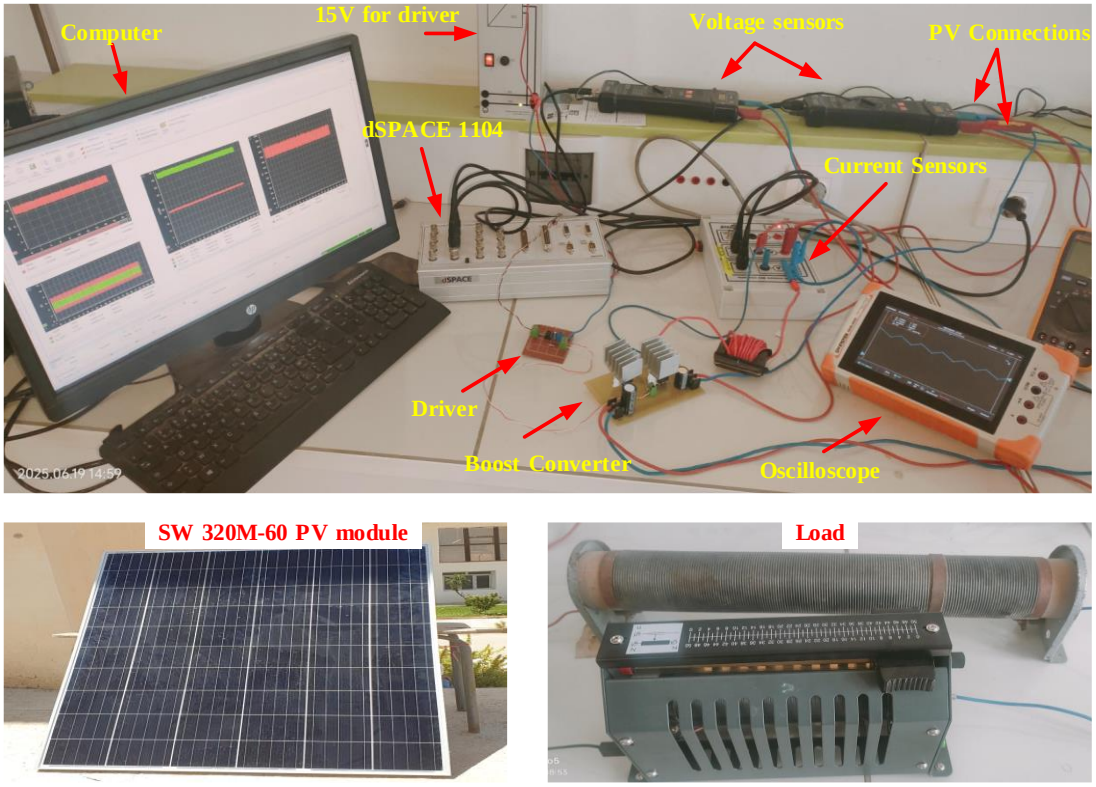

Figure III-13 Photograph of the Experimental Test Bench for MPPT Control

III.5.1.1 dSPACE Implementation and Data Acquisition

The implementation of the MPPT algorithms relies on creating a control model (.sdf file) in MATLAB/Simulink. For robust interfacing, signals acquired by the dSPACE ADC are passed through a gain block before being monitored in ControlDesk, while output signals are passed through an attenuating gain block. The sampling time for the dSPACE controller is a critical parameter and must be set as a multiple of the system's switching period ($\frac{1}{f_d}$).

Real-time monitoring and data capture were performed using dSPACE ControlDesk. The "Recorder" tool proved invaluable for capturing data points into vectors, which were then saved as .mat files for detailed post-analysis in MATLAB.

It was through this recorded data that a key real-world observation was confirmed: the actual power generated by the SW320M-60 panel (peaking around 200W) is significantly less than its rated power of 320W. This discrepancy is expected and is due to the difference between real-world operating conditions (solar irradiance and temperature in Algeria) and the ideal Standard Test Conditions (STC) under which panels are rated.

III.5.1.2 Practical direct MPP

The direct Perturb & Observe (PO) MPPT algorithm was first implemented. The Simulink model, detailing the signal flow from sensor inputs (ADCs) to the MPPT logic and PWM generation for the boost converter, is shown in Figure III-14.

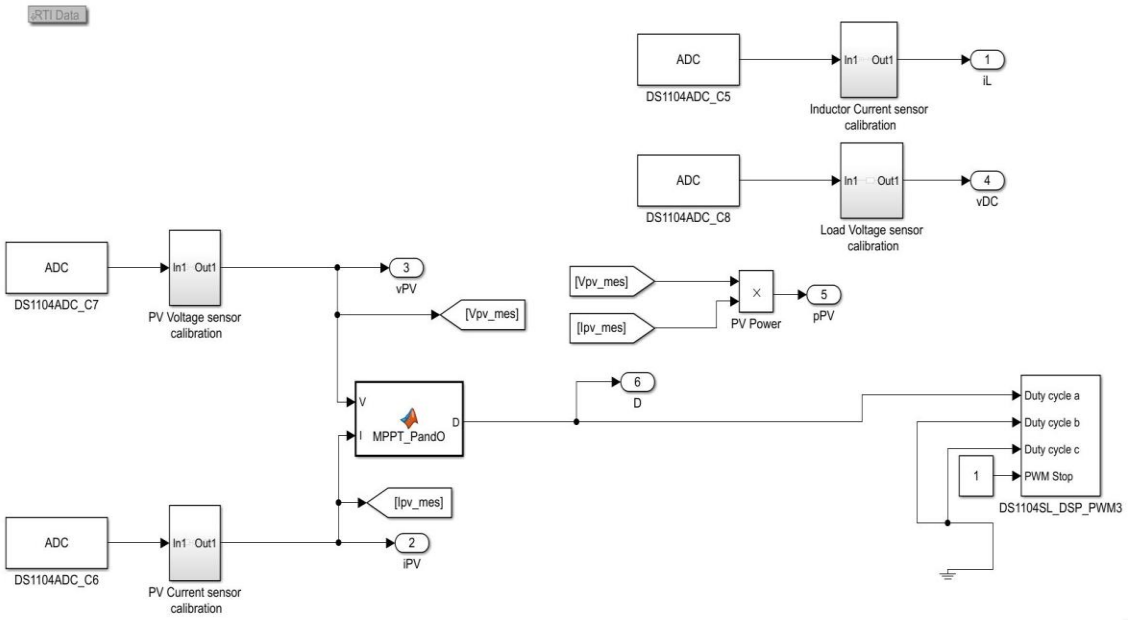

Figure III-14 Simulink Implementation of the Direct Perturb & Observe (PO) MPPT Algorithm for dSPACE DS1104 Deployment.

The first test involved a direct MPPT method, identified as a Perturb & Observe (PO) algorithm. The experimental results for this test (Wednesday, May 28, 2025, 3:31:29 PM) are shown in Figure III-15. The plots demonstrate the algorithm's dynamic tracking behavior. As seen in Figure III-15 (d), the controller successfully located and tracked the MPP, achieving an average power output of approximately 200 W.

The corresponding PV voltage and current, shown in Figure III-15 (c) and (b), settled around 27.5 V and 6.8 A, respectively. The characteristic oscillations visible in the plots for power, voltage, and current are inherent to the PO method, as it continuously perturbs the operating point to ensure it remains at the peak. These results validate the successful implementation of the direct PO controller.

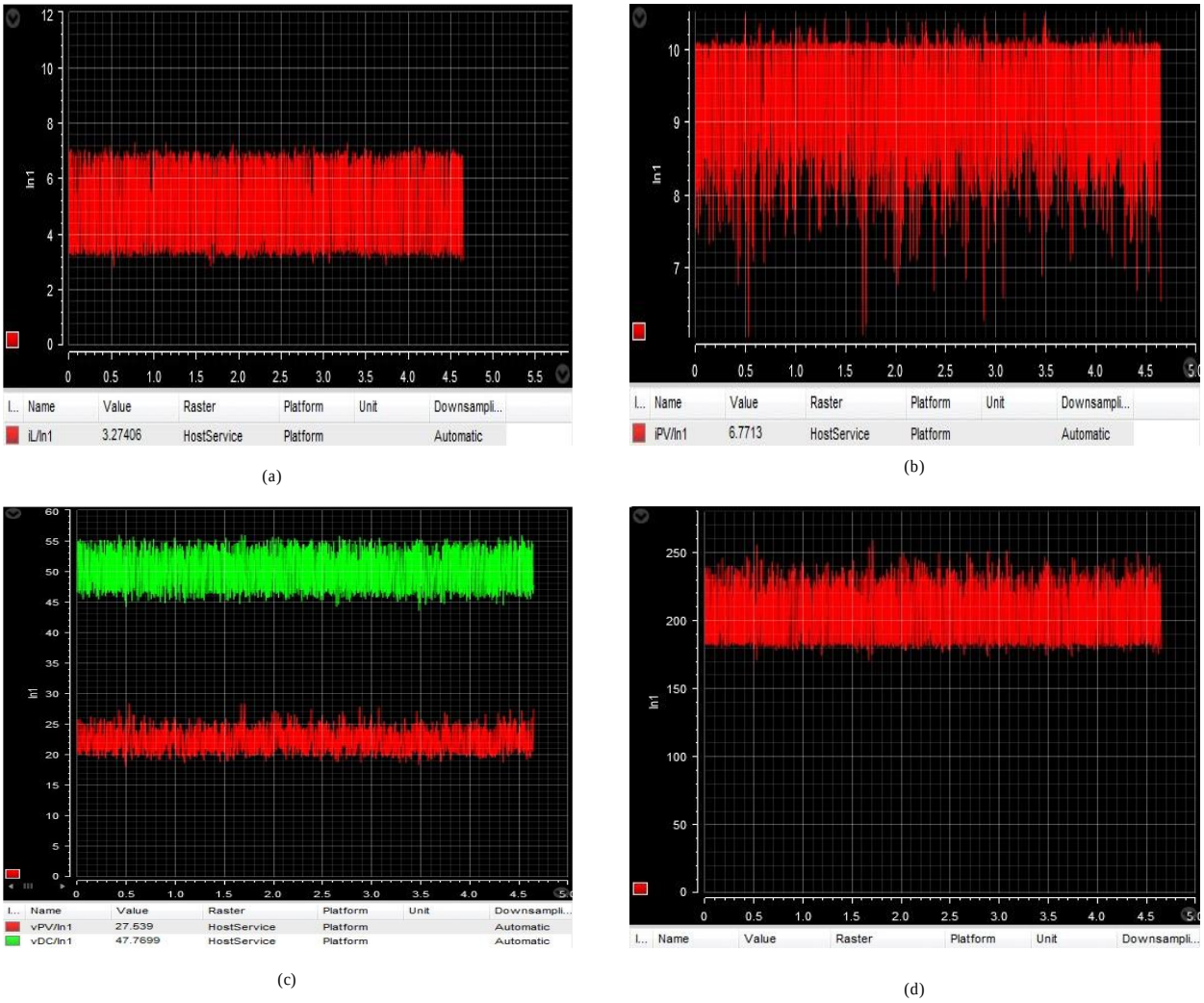

Figure III-15 Experimental Tracking of the MPP (in Control Desk) using direct PO of :

a) Inductance Current (i_L), b) PV Current (i_{PV}), c) PV Voltage (v_{PV}) and Load Voltage (v_{DC}), d) PV Power (p_{PV})

III.5.1.3 Practical Control MPP Method

Next, a Control MPPT Method strategy, also based on PO logic but incorporating a control loop to track a reference voltage, was evaluated. The corresponding Simulink model illustrating this approach is presented in Figure III-16.

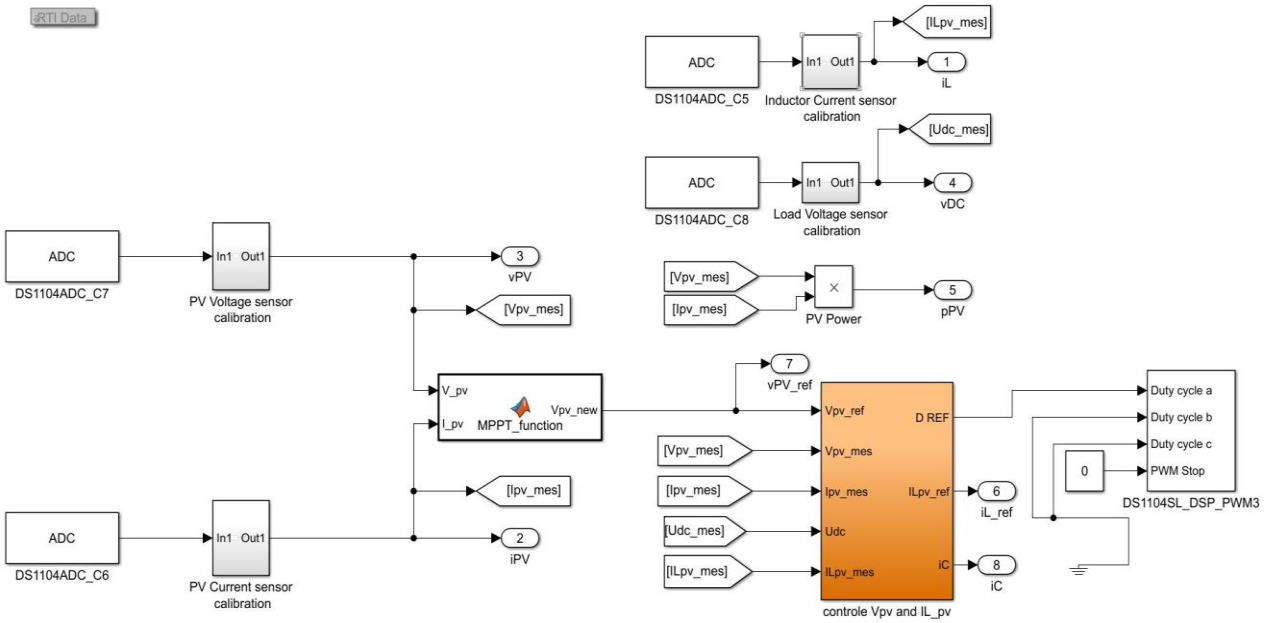

Figure III-16 Simulink Implementation of the Control of MPPT Method Perturb & Observe (PO) Algorithm with Voltage Reference Tracking for dSPACE DS1104 Deployment.

In this approach, the Control MPPT Method strategy was evaluated (Wednesday, May 28, 2025, 4:00:55 PM). The controller tracks a reference value—in this case, derived from a Control MPPT Method PO logic—to maintain the system at the MPP. The results of this experiment are presented in Figure III-17.

As shown in Figure III-17 (d), this method achieved a stable average power output of approximately 200 W, which is notably higher than that achieved by the direct method, likely due to slightly different and potentially more favorable irradiance conditions during this test. The system operated at an average PV voltage of 20.2 V and a PV current of 9.85 A, as seen in Figure III-17 (c) and (b). The results demonstrate that the Control MPPT Method scheme is also highly effective, providing stable and efficient power extraction. The comparison between the two methods highlights the performance trade-offs inherent in different MPPT strategies under real-world dynamic conditions.

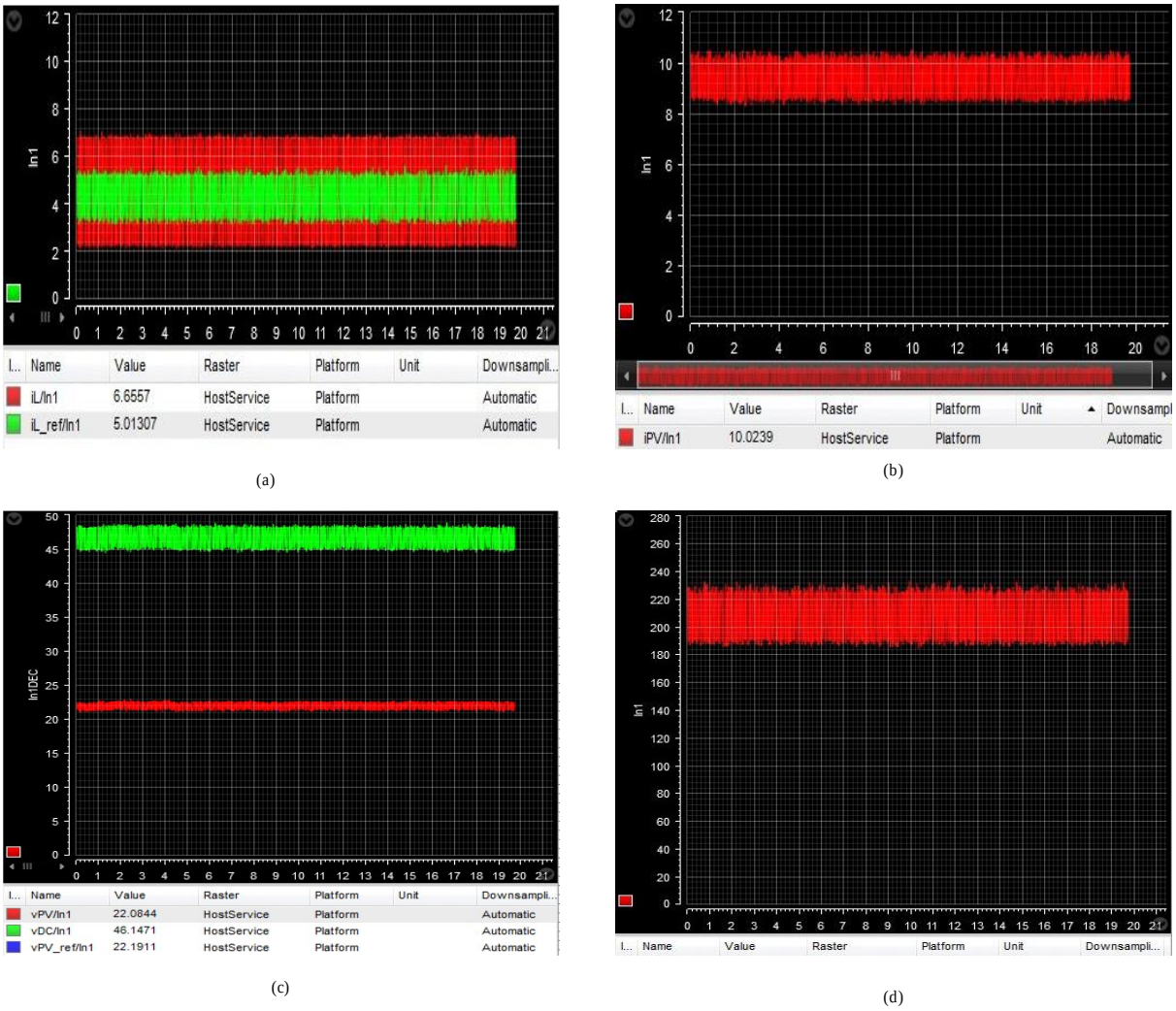

Figure III-17 Experimental Tracking of the MPP (in Control Desk) using Control MPPT Method PO of:

a) Inductance Current Reference (iL_ref), b) PV Current (iPV), c) PV Voltage (vPV), Load Voltage (v_{DC}) and PV Voltage Reference (v_{PV_ref}), d) PV Power (p_{PV})

III.6 Conclusion

While effective, the Control MPPT PO Method presented implementation challenges. It is a complex algorithm requiring numerous sensors, and it was noted that the circuit's capacitance can influence the tracked power by affecting the inductor current, highlighting a potential area for optimization.

This chapter successfully transitioned from theoretical analysis to practical, hands-on validation of Maximum Power Point Tracking (MPPT) controllers for a PV system. Through the use of a dSPACE DS1104 hardware-in-the-loop platform, the real-world performance of a custom-built boost converter and associated control algorithms was rigorously evaluated.

The initial characterization of the SW320M-60 PV module under the prevailing conditions in Algeria confirmed its non-linear I-V and P-V characteristics and demonstrated the significant impact of varying solar irradiance on power output. The peak observed power of approximately 200 W, while lower than the panel's 320W STC rating, provided a realistic baseline for the control experiments.

The design and verification of the boost converter's key components, including the 0.70 mH inductor and 470µF capacitor, were documented, linking the design principles from Chapter 2 to the physical hardware. Open-loop tests further validated the converter's ability to drive the PV module across its entire operating range, successfully locating the MPP manually and confirming the system was ready for closed-loop control.

The core of this chapter's work involved the implementation and testing of two distinct MPPT strategies: a direct and a Control of MPPT Method Perturb & Observe (PO) algorithm. Both methods proved effective at automatically tracking the maximum power point. The direct PO controller successfully maintained operation at the MPP, achieving an average power of around 200 W, though with the characteristic oscillations inherent to the method. The Control PO Method controller also demonstrated highly effective and stable power extraction, achieving a similar power output under slightly different irradiance conditions.

Ultimately, this chapter validates the efficacy of the developed control schemes in a near-real-world environment. It successfully bridged the gap between simulation and tangible performance, confirming that both the direct and Control MPPT Method controllers, when implemented on the dSPACE platform, are capable of robust and efficient power harvesting from a PV module. The experimental results and practical insights gained have laid a solid foundation for the real-world application of these MPPT systems.

General Conclusion

IV. General Conclusion

This thesis has successfully addressed the critical challenge of power optimization in photovoltaic systems by presenting a comprehensive framework for the design, modeling, simulation, and experimental validation of a Maximum Power Point Tracking (MPPT) control system. The work methodically bridged the gap from fundamental theory to practical hardware implementation, culminating in a robust and efficient solution for maximizing energy harvest from a photovoltaic source.

The investigation began by establishing a solid theoretical foundation, detailing the physics of the photovoltaic effect and developing an accurate single-diode model for the PV panel. This analytical groundwork was essential for understanding the non-linear I-V and P-V characteristics that make power optimization a non-trivial problem. Subsequently, the power electronic interface; the DC-DC boost converter was rigorously modeled using the state space averaging method. A key contribution of the simulation phase was the comparative evaluation of two Perturb and Observe (PO) control strategies: a direct control method and a control of MPPT method (cascaded PI). Simulation results in MATLAB clearly demonstrated that while both methods could track the Maximum Power Point (MPP), the cascaded control architecture exhibited vastly superior dynamic performance and robustness, particularly in its ability to reject sudden load disturbances with minimal impact on the PV source.

The crucial transition from simulation to practice was accomplished through experimental validation using a dSPACE DS1104 controller. A physical test bench, incorporating a SW320M-60 PV module and a custom-built boost converter, was used to test the control algorithms in a real-world environment. The experimental results provided a definitive validation of the simulation findings. Both direct and control of MPPT method successfully tracked the MPP, achieving an average power output of approximately 200 W under prevailing atmospheric conditions.

In totality, this thesis presents a complete and cohesive framework for the analysis and implementation of an efficient MPPT system. By successfully integrating theoretical principles with practical power electronics and control engineering, this work provides a validated roadmap for developing high-performance solar energy conversion systems. The findings confirm that a well-designed cascaded control structure offers significant advantages over direct control methods, ensuring maximum power extraction even under dynamic operating conditions.

While this study successfully achieved its objectives, it also opens avenues for future research. The developed experimental platform is well-suited for implementing and comparing more advanced MPPT algorithms, such as Incremental Conductance or intelligent controllers based on Fuzzy Logic, particularly under more complex scenarios like partial shading. Further optimization of the boost converter components and exploration of different converter topologies could also yield additional improvements in overall system efficiency.

Appendix

Table C Characteristics of the SW320M-60 (320W) Photovoltaic Module [10]

Mechanical parameters

Cell(mm)	158.75*158.75
Weight(kg)	19 (Approx)
Glass Thickness	3.2mm
Dimensions (L*W*H)(mm)	1665*1002*35mm
Cable Cross Section Size (mm²)	4
Cable Cross Section Length (mm)	900/1200
No.of Cells and Connections	60(6*10)
Junction Box	≥IP67
Connector	MC4 Compatiple

Working Conditions

Maximum System Voltage	DC 1500V
Operating Temperature	-40℃~ +85℃
Maximum Series Fuse	15A
Maximum Static Load,Front (e.g.,snow and wind)	5400Pa (112 lb/ft²)
Maximum Static Load,Back (e.g.,wind)	2400Pa (50 lb/ft²)
NOCT	45±2℃
Positive power tolerance	0~ +5W
Application Class	Class A

Engineering Drawings

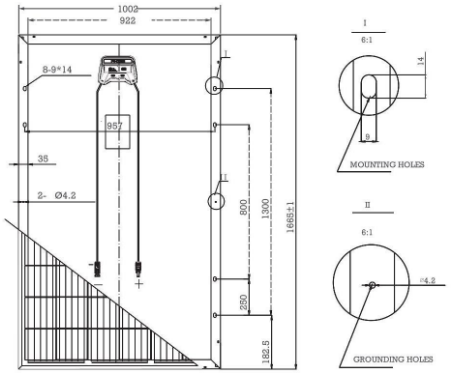

Packaging Configuration

Moduels Per Pallet	31Pcs
Moduels Per 20GP	412Pcs
Moduels Per 40HQ	952Pcs

Electrical Parameters

Module	SW320M-60 ~ SW360M-60				
Encapsulation	Class/Eva/Cell/Eva/Backsheet				
Maximum Power Pmax (W)	320	330	340	350	360
Maximum Power Voltage (Vmp/V)	33.40	33.80	34.20	34.60	34.80
Maximum Power Current (Imp/A)	9.58	9.76	9.94	10.12	10.30
Open Circuit Voltage (Voc/V)	41.00	41.60	42.20	42.80	43.40
Short Circuit Current (Isc/A)	10.14	10.30	10.46	10.62	10.78
Cell Efficiency(%)	21.16	21.82	22.50	23.15	23.81
Module Efficiency (%)	19.18	19.78	20.38	20.98	21.58
Power Tolerance (W)	0 ~ +5W				
Temperature Coefficient of Isc (αIsc)	+0.059%/℃				
Temperature Coefficient of Voc (βVoc)	-0.330%/℃				
Temperature Coefficient of Pmax (γPmp)	-0.410%/℃				
STC	Irradiance 1000W/㎡, Cell Temperature 25℃, Air Mass 1.5				

I-V Curve

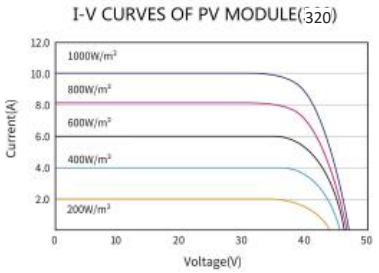

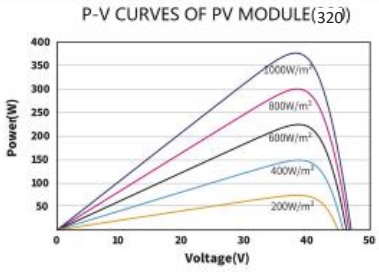

Table D Electrical Characteristics of the Toshiba 50JR22 IGBT

Characteristics			Symbol	Rating	Unit
Collector-emitter voltage			V_{CES}	600	V
Gate-emitter voltage			V_{GES}	±25	
Collector current (DC)	(T_c = 25°C)		I_C	50	A
Collector current (DC)	(T_c = 100°C)			44	
Collector current (1 ms)			I_{CP}	100	
Diode forward current (DC)			I_F	40	
Diode forward current (100 μs)			I_{FP}	100	
Collector power dissipation	(T_c = 25°C)		P_C	230	W
Collector power dissipation	(T_c = 100°C)			115	
Junction temperature		(Note 1)	T_j	175	°C
Storage temperature			T_{stg}	-55 to 175	
Mounting torque			TOR	0.8	N · m

Note: Using continuously under heavy loads (e.g. the application of high temperature/current/voltage and the significant change in temperature, etc.) may cause this product to decrease in the reliability significantly even if the operating conditions (i.e. operating temperature/current/voltage, etc.) are within the absolute maximum ratings.
Please design the appropriate reliability upon reviewing the Toshiba Semiconductor Reliability Handbook ("Handling Precautions"/"Derating Concept and Methods") and individual reliability data (i.e. reliability test report and estimated failure rate, etc).

In general, loss of IGBT increases more when it has positive temperature coefficient and gets higher temperature.
In case that the temperature rise due to loss of IGBT exceeds the heat release capacity of a device, it leads to thermorunaway and results in destruction.
Therefore, please design heat release of a device with due consideration to the temperature rise of IGBT.

Note 1: Ensure that the junction temperature does not exceed 175°C.

References

[1] M. L. Katche, A. B. Makokha, S. O. Zachary, and M. S. Adaramola, "A Comprehensive Review of Maximum Power Point Tracking (MPPT) Techniques Used in Solar PV Systems," Mar. 01, 2023, *MDPI*. doi: 10.3390/en16052206.

[2] M. A. Green, *Solar Cells: Operating Principles, Technology, and System Applications*. in Prentice-Hall Series in Solid State Physical Electronics. Englewood Cliffs, NJ: Prentice-Hall, Inc., 1982.

[3] M. G. Villalva, J. R. Gazoli, and E. R. Filho, "Comprehensive approach to modeling and simulation of photovoltaic arrays," *IEEE Trans Power Electron*, vol. 24, no. 5, pp. 1198–1208, 2009, doi: 10.1109/TPEL.2009.2013862.

[4] B. Bendib, H. Belmili, and F. Krim, "A survey of the most used MPPT methods: Conventional and advanced algorithms applied for photovoltaic systems," 2015, *Elsevier Ltd.* doi: 10.1016/j.rser.2015.02.009.

[5] R. A. Messenger and J. Ventre, *Photovoltaic Systems Engineering*, Third. Boca Raton, FL: CRC Press, Taylor & Francis Group, 2010. doi: 10.1201/9781439802939.

[6] T. Esram and P. L. Chapman, "Comparison of photovoltaic array maximum power point tracking techniques," *IEEE Transactions on Energy Conversion*, vol. 22, no. 2, pp. 439–449, Jun. 2007, doi: 10.1109/TEC.2006.874230.

[7] C. Honsberg and S. Bowden, "Effect of Temperature," 2019.

[8] S. Azimi-Nam and F. Farhani, "Effect of Temperature on Electrical Parameters of Phosphorous Spin-on Diffusion of Polysilicon Solar Cells," *Journal of Renewable Energy and Environment*, vol. 4, no. 1, pp. 41–45, 2017, doi: 10.22059/jree.2017.64332.

[9] K. Muthukumar and T. S. Anandhi, "Real time implementation of variable step size based P&O MPPT for PV systems based on dSPACE," *International Journal of Power Electronics and Drive Systems*, vol. 7, no. 3, pp. 915–925, Sep. 2016, doi: 10.11591/ijpeds.v7.i3.pp915-925.

[10] Sunway Solar Energy Tech. Co. Ltd., "SW360M-60 Monocrystalline 60 Cells 320W-360W," 2022.

[11] S. S. Ang and A. R. Oliva, *Power-Switching Converters*, Second. Boca Raton, FL: CRC Press, 2005. doi: 10.1201/9781420029009.

[12] S. A. Kalogirou, "Solar Energy Engineering Processes and Systems Second Edition." [Online]. Available: http://store.elsevier.com/

[13] M. S. Bouakkaz, "Contribution to the Study and Modelling of Photovoltaic System Dynamic Behaviour," Ph.D. dissertation, University of August 20th, 1955, Skikda, 2020.

[14] A. K. Singh, T. Tariq, M. F. Ahmer, G. Sharma, P. N. Bokoro, and T. Shongwe, "Intelligent Control of Irrigation Systems Using Fuzzy Logic Controller," *Energies (Basel)*, vol. 15, no. 19, Oct. 2022, doi: 10.3390/en15197199.

References

[15] S. Djeriou, "Performance Improvement of Photovoltaic Pumping System," University M'Hamed Bougara Boumerdes, Institute of Electrical and Electronic Engineering, Boumerdes, Algeria, 2018.

[16] S. Motahhir, A. El Ghzizal, S. Sebti, and A. Derouich, "MIL and SIL and PIL tests for MPPT algorithm," *Cogent Eng*, vol. 4, no. 1, p. 1378475, 2017, doi: 10.1080/23311916.2017.1378475.

[17] M. S. Habitouche and I. Sahli, "Etude et conception d'une commande non linéaire appliquée au convertisseur statique DC-DC," Université Mohamed El Bachir El Ibrahimi - Bordj Bou Arréridj, Faculté des Sciences et de la Technologie, Département d'Electromécanique, Bordj Bou Arréridj, Algérie, 2021.

[18] "DS1104 R&D Controller Board Hardware Installation and Configuration: For DS1104 and CP1104/CLP1104 Connector Panels," Mar. 2004.